https://doi.org/10.5194/gmd-2021-118
Preprint. Discussion started: 16 June 2021

Geoscientific Model Development Discussions

SIMO v1.0: Simplified model of the vertical temperature profile in a small warm monomictic lake

Kristina Šarović[1], Zvjezdana B. Klaić[1]

[1]Department of Geophysics, Faculty of Science, University of Zagreb, Zagreb, 10000, Croatia

Correspondence to: Kristina Šarović (kristina.sarovic@gmail.com)

Abstract. A simple 1-D energy budget model (SIMO) for the prediction of the vertical temperature profiles in small, monomictic lakes forced by a reduced number of input meteorological variables is proposed. The model estimates the net heat flux and thermal diffusion using only routinely measured hourly mean meteorological variables (namely, the air temperature, relative humidity, atmospheric pressure, wind speed, and precipitation), hourly mean ultraviolet B radiation (UVB), and climatological monthly mean cloudiness data. Except for the initial vertical temperature profile, the model does not use any lake-specific variables. The model performance was evaluated against lake temperatures measured continuously during an observational campaign in two lakes belonging to the Plitvice Lakes, Croatia (Lake 1 and Lake 12). Temperatures were measured at 15 and 16 depths ranging from 0.2 to 27 in Lake 1 (maximum depth of 37.4 m) and 0.2 to 43 m in Lake 12 (maximum depth of 46 m). A sensitivity analysis of the simulation length was performed for simulation lengths from 1 to 30 days. The model performed reasonably well and it was able to satisfactorily reproduce the vertical temperature profile at the hourly scale, the deepening of the thermocline with time, and the annual variation in the vertical temperature profile. A yearlong simulation initiated with an approximately constant vertical profile of the lake temperature (≈ 4°C) was able to reproduce the onset of stratification and convective overturn. However, the thermocline depth was underestimated while the epilimnion temperatures were overestimated. Nevertheless, the values of the model performance measures obtained for a yearlong simulation were comparable with those reported for other more complex models. Thus, the presented model can be used for the assessment of the onset and duration of lake stratification periods when water temperature data are unavailable, which can be useful for various lake studies performed in other scientific fields, such as biology, geochemistry, and sedimentology.

1 Introduction

Water temperature is a critical factor that directly influences a whole range of lake properties. It controls the solubility of gases and minerals, the rate of chemical reactions, and biological activity and diversity (e.g., Benson and Krause, 1980; Rasconi et al., 2017; Krumgalz, 2018). In addition, the vertical temperature profile in a lake (and consequent lake stratification/water column stability) and the length of the stratification period play a vital role in the transport pathways of gases and nutrients and, consequently, their distribution within a lake (e.g., Vachon et al., 2019; Ladwig et al., 2021). Furthermore, there is a two-way interaction between lakes and the atmosphere. While the thermodynamic behavior of lakes is mainly driven by

https://doi.org/10.5194/gmd-2021-118
Preprint. Discussion started: 16 June 2021


Geoscientific Model Development Discussions

meteorological conditions, the distinct physical features of lakes (such as surface roughness, albedo, heat capacity/temperature, and evaporation rate) introduce surface heterogeneity in the domain of interest. Thus, their presence modifies surface-atmosphere fluxes and local and regional weather and climate (e.g., MacKay, 2012; Klaić and Kvakić, 2014; Brian et al., 2015; Kristovich et al., 2017; Wu et al., 2019). Thus, over the last couple of decades, increasing scientific interest has been focused on both modeling the thermal regime of lakes (e.g., Stepanenko et al., 2013, 2016; Thiery et al., 2014; MacKay et al., 2017) and its sensitivity to climate change (e.g., Vinnå et al., 2021).

Due to their relative simplicity and computational efficiency, there is a widespread use of one-dimensional (1-D) water temperature prediction models. There are different types of 1-D models of varying complexity, although they can generally be divided into three groups: (1) mixed layer (usually two-layer) models based on the energy-budget approach, (2) differential models based on solving the 1-D heat transfer equation (thermal diffusivity models), and (3) second-order turbulence closure models. Energy budget-based models assume two distinct well-mixed layers, namely, the epilimnion and hypolimnion, and they use the kinetic energy produced by wind shear on the surface to account for the mixing dynamics within these two layers and/or to estimate the depths of these layers (e.g., Bell et al., 2006; Mironov et al., 2010; Hipsey et al., 2019). Thermal diffusivity-based models usually consist of many well-mixed layers for which the heat transfer equation is solved (e.g., Hostetler and Bartlein, 1990; Liston and Hall, 1995; Stefan et al., 1998; Sun et al., 2007). The second-order turbulence closure models are also known as k-ε, where k is the turbulent kinetic energy per unit mass and ε is the turbulent kinetic energy dissipation rate (e.g., Goudsmit et al., 2002). They solve the turbulent kinetic energy transport equation and are computationally considerably more expensive than the previous two types (e.g., Goudsmit et al., 2002; Stepanenko et al., 2011, 2014).

Except in the basic underlying approach, lake models differ in the processes they include, such as wind sheltering, sediment heat flux, attenuation of light, phase change, convective mixing and others. Direct implementation of a particular process in a model or the simplification or even omission of the process is usually justified by the model purpose. Lake models are developed for various purposes, including improvement of numerical weather prediction and climate models (e.g., Mirnov et al, 2010; MacKay, 2012), evaluation of the effects of climate change (e.g., Stefan et al., 1998; Wu et al., 2020, Vinnå et al., 2021), or facilitation of specific limnological studies. Some of these specific studies address gas (e.g., methane and/or CO_2) emissions (e.g., Stepanenko et al., 2011), oxygen and nutrient levels (e.g., Bell et al., 2006), heat and mass exchange between the atmosphere and a water body (Sun et al., 2007), and evaporation and lake level fluctuation (Hostetler and Bartlein, 1990).

To run lake models, input data, which are generally not available from routine meteorological measurements, are needed. Specifically, these data include both shortwave and longwave radiation component data. The goal of this study is to formulate a simplified model for predicting the vertical temperature profile in a small (less than 50 m deep) warm monomictic lake, which, except for the ultraviolet B radiation (UVB) and climatological monthly mean cloudiness data, is forced solely by routinely available observed surface meteorological data (namely, the air temperature, relative humidity, atmospheric pressure, wind speed and precipitation). Conversely, other lake-temperature models that are forced with observational data (e.g., Bell et al., 2006; Sun et al., 2007; Martynov et al., 2010; MacKay, 2012, 2017) require both shortwave and longwave radiation component data. In addition, we examined the sensitivity of the proposed model performance to the length of the simulated

https://doi.org/10.5194/gmd-2021-118
Preprint. Discussion started: 16 June 2021

time interval. To the best of our knowledge, such a detailed evaluation has not been reported in previous lake-temperature modeling studies. Since vertical temperature profiles in lakes are not routinely measured, we also addressed the ability of the proposed model to simulate the onset and termination of lake stratification by a yearlong simulation initiated with a uniform temperature over a completely mixed water column. A similar study was performed by Martynov et al. (2010) for two small dimictic lakes in the USA using an eddy diffusivity model and a two-layer model, Goudsmit et al. (2002) analyzed the performance of a k-ε model in a two-year length simulation, while Bruce et al. (2018) analyzed a set of 32 lakes all over the globe using the General Lake Model (GLM). All of these models are more complex and/or require more extensive input data than the one proposed in this study.

The model proposed here is evaluated using lake-temperature experimental data measured at two lakes of the Plitvice Lakes, Croatia. Details about the study area and data collection are presented in Section 2. The model's governing equations and parametrizations used are described in Section 3. Measures of the model performance and evaluation approach are described in Section 4. The results are presented and discussed in Section 5. Finally, a short summary and conclusions are given in Section 6.

2 Study area and measurements

2.1. Study area

Plitvice Lakes is a karstic lake system situated in the mountainous region of Croatia (Fig. 1). The system consists of 16 named and several smaller unnamed lakes. The lakes are interconnected with cascades and waterfalls, making an approximately 9 km long chain extending in roughly a south-north direction. With its unique geomorphology and exceptional biodiversity, the area has been a subject of scientific research dating as early as 1850 (NPPL, 2021). An extensive multidisciplinary overview of abiotic studies focusing on the Plitvice Lakes area is provided by Klaić et al. (2018).

The numerical model proposed in this paper was applied to the two largest lakes of the system, Prošće and Kozjak Lakes (Fig. 1c and d). Prošće Lake (hereafter Lake 1) is the southernmost and the first lake in the system. The lake altitude, area, maximum and average depth, and volume are 636.6 m above sea level (ASL), 0.68 km^2, 37.4 m, 13.2 m, and 0.00767 km^3, respectively. Kozjak Lake (hereafter Lake 12) is the 12th lake in the chain at an altitude of 535 m ASL. It is the largest and deepest lake in the system, with maximum and average depths of 46 and 17.3 m, respectively, a surface area of 0.82 km^2, and a volume of 0.01271 km^3. Based on their surface areas, both lakes can be considered small (e.g., Forcat et al., 2011).

2.2. Observational data

2.2.1. Lake temperatures

This study uses lake temperatures measured at two different points (Fig. 1), one in Lake 1 (point P1, φ = 44.8676 °N, λ = 15.5981 °E, 636 m ASL) and the other in Lake 12 (point K1, ϕ = 44.8902 °N, λ = 15.6038 °E, 535 m ASL). Each point was positioned in the deepest part of the corresponding lake. Lake temperatures were measured and logged with HOBO TidBiT

https://doi.org/10.5194/gmd-2021-118
Preprint. Discussion started: 16 June 2021

Geoscientific Model Development Discussions

MX Temp 400 as previously described for Lake 1 in Klaić et al. (2020b) and Lake 12 in Klaić et al. (2020a). The accuracy of the sensors is ±0.20 °C for temperatures between 0 and 70 °C and ±0.25 °C for temperatures between −20 and 0 °C. The initial sampling frequency of lake temperatures was 1 Hz, while 2-min means were stored. However, since meteorological data were available at a resolution of one hour, we used hourly mean lake temperatures in the present study.

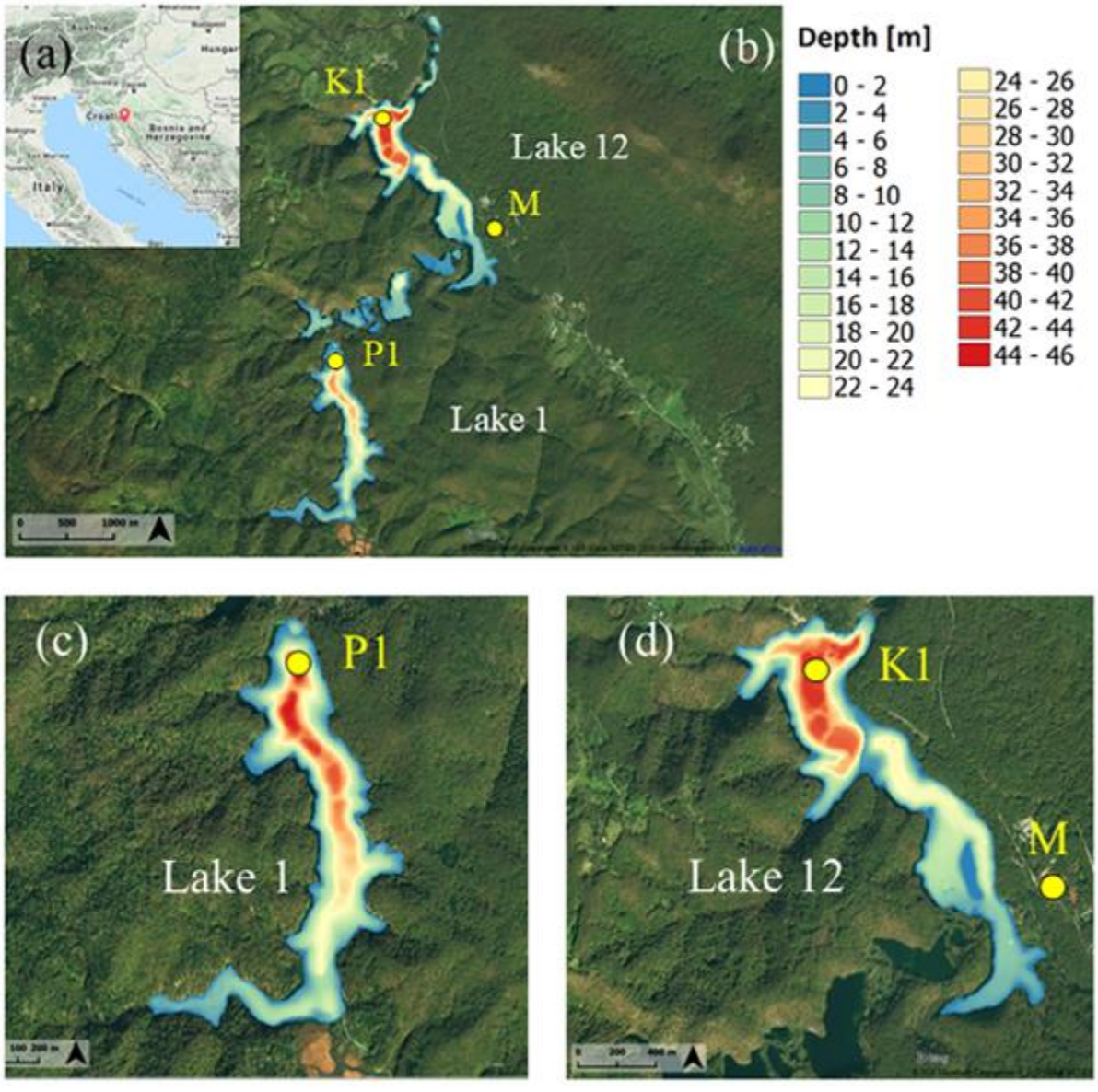

Figure 1 Location of Plitvice Lakes (red bubble; source: © Google Maps) (a). Closer look at the entire lake system (b), Lake 1 (c) and Lake 12 (d). Locations of the lake temperature measuring points P1 (φ = 44.8676°N, λ = 15.5981°E, height of the lake surface 636 m ASL) and K1 (φ = 44.8902°N, λ = 15.6038°E, 535 m ASL) and meteorological measuring site M (φ = 44.8811°N, λ = 15.6197°E, 579 m ASL) are shown with yellow circles. Panels b–d show composite pictures of the lake bathymetries and the digital orthophoto images (DOF: http://www.bing.com/maps/?v=2&app=60526, Print Rights – Under the © Microsoft® Bing™ Maps Platform APIs' Terms of Use).

https://doi.org/10.5194/gmd-2021-118
Preprint. Discussion started: 16 June 2021

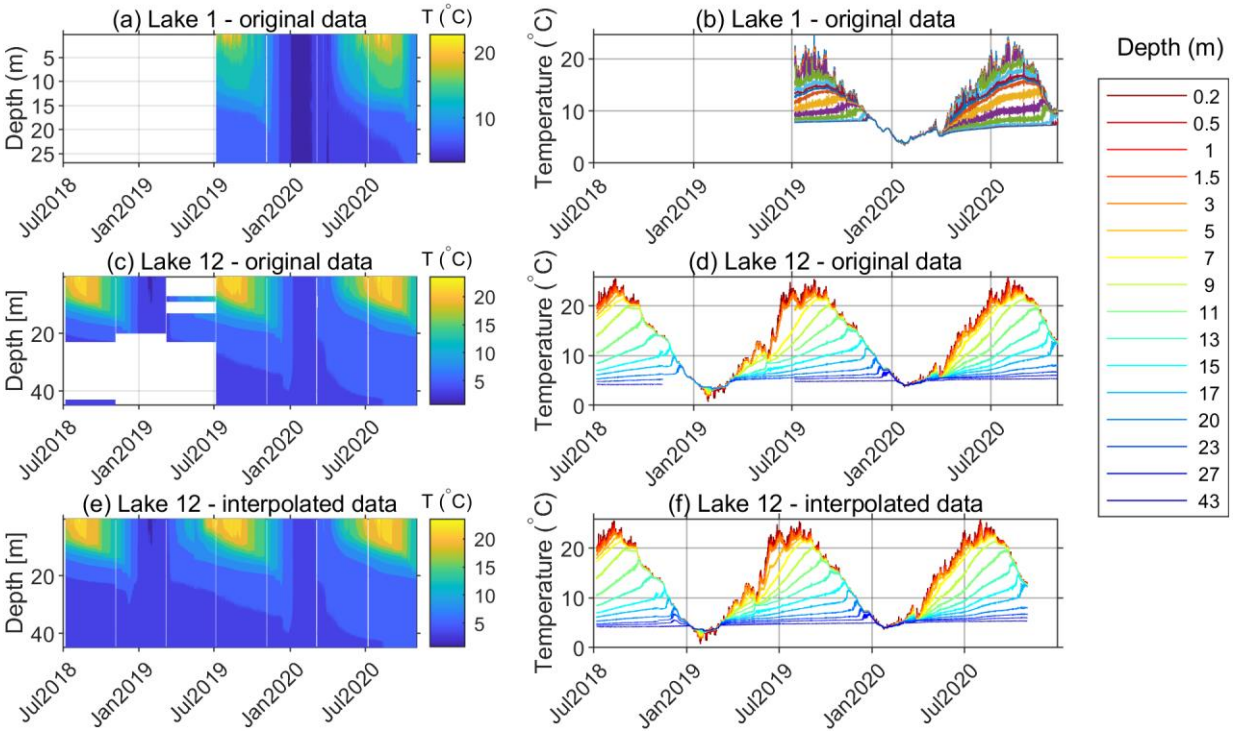

Figure 2 Measured water temperatures in Lake 1 (a and b) and Lake 12 (c and d) and water temperature in Lake 12 after interpolation of the measured data (e and f).

At site P1 (Lake 1), 15 factory-calibrated sensors were positioned at fixed depths of 0.2, 0.5, 1, 1.5, 3, 5, 7, 9, 11, 13, 15, 17, 20, 23, and 27 m. As Lake 12 is deeper than Lake 1, an additional sensor was placed at a depth of 43 m at site K1 together with 15 sensors at the same depths as at site P1.

The temperature recording started on 7 July 2018 at K1 and 6 July 2019 at P1 (Table 1). Temperatures were recorded continuously except during several short periods (≈ 1–2 days, once in approximately four months) when the sensors were pulled out of the lakes for the purpose of data acquisition. These periods without measurements are shown as thin vertical white lines in Fig. 2a, c and e. Due to the malfunction of some sensors during the first year of the measurement campaign, data for some observational depths at K1 are missing. Missing data are shown as white areas from July 2018 to July 2019 in Fig. 2c or as intermitted lines in Fig. 2d. The inoperative sensors were later replaced. Missing data at specific depths were subsequently replaced by data calculated by spatial linear interpolation from the two adjacent depths using existing data (Fig. 2e and f). However, temporal interpolation was not performed since it would fail to reproduce the temporal variability in lake temperature at particular depths during periods of data acquisition. Interpolated lake temperatures were used solely to illustrate the evolution of Lake 12 stratification (Fig. 2e), while they were omitted in the calculations of the model performance measures (Section 4).

https://doi.org/10.5194/gmd-2021-118
Preprint. Discussion started: 16 June 2021

Geoscientific Model Development Discussions

Table 1 Availability of measured data. The positions of the measuring points are shown in Fig. 1.

Data set	Measurement point	Availability of data
Water temperature	K1 (Lake 12, maximum depth 46 m) φ = 44.8902°N, λ = 15.6038°E, 535 m ASL	7 July 2018 – 2 November 2020
Water temperature	P1 (Lake 1, maximum depth 37.4 m) φ = 44.8676°N, λ = 15.5981°E, 636 m ASL	6 July 2019 – 2 November 2020
Meteorological data	M φ = 44.8811°N, λ = 15.6197°E, 579 m ASL	7 July 2018 – 4 November 2018 1 January 2019 – 31 December 2019 2 July 2020 – 30 September 2020

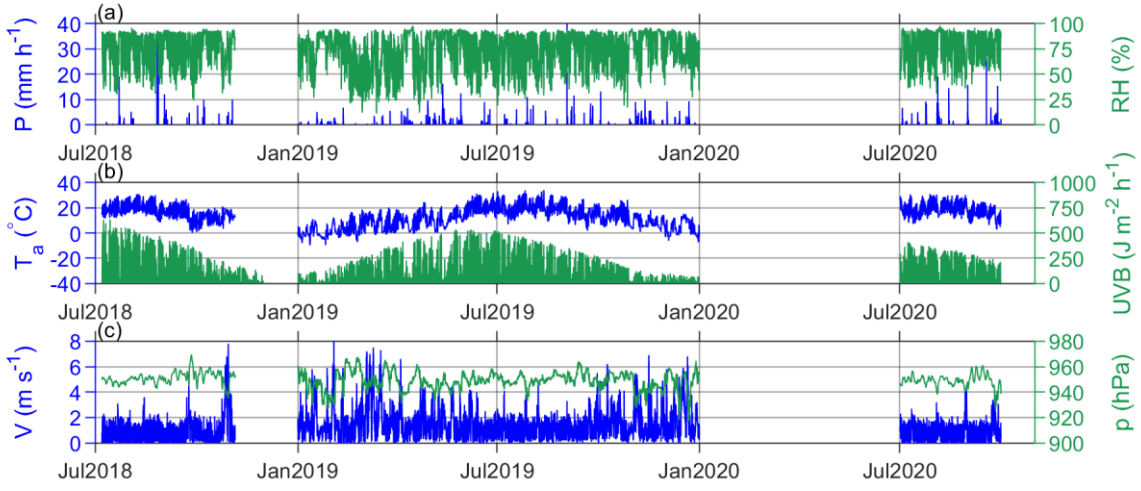

125

Figure 3 Available meteorological data from the automatic meteorological station Plitvička Jezera (φ = 44.8811°N, λ = 15.6197°E, 579 m ASL): (a) precipitation amount (P) and relative humidity (RH), (b) air temperature (T_a) and UVB radiation (UVB), and (c) wind speed (V) and atmospheric pressure (p).

2.2.2. Meteorological data

130 Meteorological data were measured at the automatic meteorological station Plitvička Jezera (point M in Fig. 1, φ = 44.8811°N, λ = 15.6197°E, altitude 579 m ASL). The station belongs to the network of the Croatian Meteorological and Hydrological Service (CMHS). The CMHS also provided quality control of these data. In the present study, we used hourly mean values of the air temperature, atmospheric pressure, UVB radiation, atmospheric relative humidity, and hourly precipitation amount measured at 2 m above ground level and wind speed measured at 10 m above ground level (Fig. 3). Wind direction data were
135 also available but were not used in the study. The station is approximately 2 km northeastward of the P1 site and 1.6 km southeastward of the K1 site. Despite the comparable distance from both the P1 and K1 sites, the meteorological conditions observed at point M are expected to be more representative for Lake 12 than for Lake 1 because this point is located at the slope adjacent to Lake 12 at approximately 200 m away from its shoreline. In addition, topographic obstacles are found

https://doi.org/10.5194/gmd-2021-118
Preprint. Discussion started: 16 June 2021


Geoscientific Model Development Discussions

between points P1 and M (Fig. 1b) and the altitude difference between P1 and M is higher than the difference between K1 and M (Table 1).

3 Model description and governing equations

The model is based on the one-dimensional energy balance equation used in similar liquid water models (e.g., Hostetler and Bartlein, 1990; Liston and Hall, 1995; Sun et al. 2007). Because ice was not observed on the two lakes during the measurement campaign (Fig. 2a and c), ice formation was not addressed in the present study. Thus, a simplified approach using water temperature instead of enthalpy is used. Assuming that the water body has a constant horizontal cross-sectional area (which can be of any shape), we come to the following equation:

$$c_p \rho \frac{\partial T}{\partial t} = \frac{\partial}{\partial z}\left\{\left[k_m + k_t\right]\frac{\partial T}{\partial z}\right\} - \frac{\partial \varphi}{\partial z} + M_{conv}\,, \tag{1}$$

where c_p is the water specific heat capacity (J kg^{-1} K^{-1}), ρ is the water density (kg m^{-3}), T is the water temperature (°C), t is time (s), z is depth (m), k_m and k_t are the molecular and turbulent thermal conductivity (W m^{-1} K^{-1}), ϕ is the heat source term (W m^{-2}) and M_{conv} is the convective mixing term (W m^{-3}).

The water density is calculated from the formula for freshwater (e.g., Sun et al., 2007):

$$\rho = \left(1 - 1.9549 \times 10^{-5}\left|T - 3.85\right|^{1.68}\right) \times 10^3\,. \tag{2}$$

The molecular thermal conductivity of water is 0.6 W m^{-1} K^{-1} (e.g., Sun et al., 2007). The turbulent thermal conductivity is a function of time and depth because it depends on meteorological forcing. Here, we also follow the method of Henderson-Sellers (1985), where the turbulent thermal conductivity is calculated as follows:

$$k_t(z) = c_p \rho\left(ku*/Pr_0\right)\exp\left(-k*z\right)\left(1 + 37\,Ri^2\right)^{-1}, \tag{3}$$

where $k = 0.4$ is the von Karman constant, $u*$ is the friction velocity at the surface (m s^{-1}), $k*$ is the latitude-dependent parameter of the Ekman profile, $Pr_0 = 1$ is the neutral value of the turbulent Prandtl number and Ri is the Richardson number. The Ekman profile parameter and the Richardson number are calculated as in Sun et al. (2007):

$$k* = 6.6\left(\sin\varphi\right)^{1/2} U_2^{-1.84}\,, \tag{4}$$

where φ is the latitude and U_2 is the wind speed at 2 m above the water surface (m s^{-1}), and

$$Ri = \frac{-1 + \left\{1 + 40\,N^2 k^2 z^2 / \left[u*^2 \exp\left(-2k*z\right)\right]\right\}^{1/2}}{20}, \tag{5}$$

where N is the Brunt-Vaisala frequency (s^{-1}):

$$N = \left[g/\rho\left(\partial\rho/\partial z\right)\right]^{1/2}. \tag{6}$$

The wind speed U_2 is determined from the logarithmic formula:

https://doi.org/10.5194/gmd-2021-118
Preprint. Discussion started: 16 June 2021


Geoscientific Model Development Discussions

$$U_2 = u^* \log(2/z_0)/k\,, \tag{7}$$

where z_0 is the roughness length (m). The air shear velocity u^* and the roughness length z_0 are calculated as in Verburg and Antenucci (2010).

Sun et al. (2007) suggest that for shallow lakes (less than 50 m deep), the turbulent thermal conductivity is negligible. Both Lake 1 and Lake 12 are less than 50 m deep (Table 1). However, as the depth of Lake 12 (46 m) is rather close to the upper depth threshold for shallow water bodies as defined by Sun et al. (i.e., the shallow lake is deeper than 10 m and shallower than 50 m; Sun et al., 2007), in the present study, turbulent thermal diffusion was taken into account using Eq. (3).

3.1. Energy budget and boundary conditions

In addition to turbulent thermal diffusion, the only other term in Eq. (1) accounting for meteorological forcing is the heat source term. The surface net heat flux consists of the net shortwave radiation (S_n), net longwave radiation (L_n), sensible heat flux (H_s), latent heat flux (H_l), and heat flux brought by precipitation (H_p). The surface boundary condition can be written as follows:

$$\phi(0) = S_n + L_n + H_s + H_l + H_p\,. \tag{8}$$

At the bottom, it is assumed that there is no heat flux and that the temperature gradient equals zero, meaning there is no heat diffusion either. Thus, the bottom boundary conditions can be written as follows:

$$\frac{\partial T}{\partial z}(z_{\max}) = 0\,, \tag{9}$$

$$\phi(z_{\max}) = 0\,. \tag{10}$$

All heat flux terms in Eq. (8) are defined to be positive when downward. Shortwave and longwave radiation measurements are not very common, and sensible and latent heat fluxes cannot be measured directly (Brunel, 1989; Bahr et al., 2012). Thus, obtaining the heat flux terms in Eq. (8) is expensive and complicated. Therefore, methods for calculating each term using commonly available meteorological data only are proposed in sections from 3.1.1. to 3.1.4.

3.1.1. Shortwave radiation

As previously indicated by other authors (e.g., Bell et al., 2006; Martynov et al., 2010; MacKay, 2012), sufficient radiation data (both shortwave and longwave) are not generally available from routine meteorological measurements, and this is also the case for meteorological station M, where only UVB radiation was measured. A number of studies provide correlations among UVA, UVB, total UV, or global solar radiation (G) (Kudish and Evseev, 2000; Kudish et al., 2005; Podstawczynska, 2009; Pokhrel and Bhattarai, 2012; Pashiardis et al., 2017) and show that significant variability occurs in the UV/G ratio between sites, which is mainly due to local atmospheric conditions. Podstawczynska (2009) indicated that air turbidity and cloudiness are the two main factors that determine the variability of daily solar energy transmission through the atmosphere.

https://doi.org/10.5194/gmd-2021-118
Preprint. Discussion started: 16 June 2021


Geoscientific Model Development Discussions

Pashiardis et al. (2017) found that the UV/G ratio increases with solar elevation and that the presence of clouds reduces the UV component less than the global solar radiation due to the strong absorption of water in the near infrared spectrum.

Winslow et al. (2001) proposed a model for estimating the total daily solar irradiance from daily precipitation and minimum and maximum temperatures, along with latitude, elevation, and mean annual temperature. This model showed significant improvement over the widely used empirical Bristow and Campbell (1984) model and was applicable for a wide range of climates. Therefore, it is also used in this study.

According to Winslow et al. (2001), the daily solar irradiance at the Earth's surface is equal to

$$S_{n\_day} = \tau_{cf} D\left(1 - \beta e_s(T_{\min}) / e_s(T_{\max})\right) S_{top}, \tag{11}$$

where S_{n_day} is the total daily solar irradiance (J m^{-2} day^{-1}), τ_{cf} is the cloud-free atmospheric transmittance, β is an additional parameter required to introduce variation between sites, $e_s(T_{\min})$ and $e_s(T_{\max})$ are the saturation vapor pressures (hPa) at the daily minimum and maximum air temperatures ($T_{\min}$ and $T_{\max}$), respectively, and S_{top} is the total daily solar irradiance at the top of the atmosphere (J m^{-2} day^{-1}). To calculate the saturation water pressure, we use the formula from Bolton (1980):

$$\begin{aligned} &e_s(T_a) = 0.611 \exp\left[mT_a / (n + T_a)\right] \\ &\text{for} \quad T_a > 0^\circ C \qquad m = 17.269 \qquad n = 237.7, \\ &\text{for} \quad T_a < 0^\circ C \qquad m = 21.753 \qquad n = 265.3, \end{aligned} \tag{12}$$

where T_a is the air temperature (°C). The total daily solar irradiance is calculated following Wald (2019):

$$S_{top} = S_0\left(1 + \varepsilon_{ecc}\right)\frac{3600 * 24}{\pi}\cos\varphi\cos\delta\left[\omega_s - \tan(\omega_s)\right], \tag{13}$$

where S_0 = 1 362 W m^{-2} is the solar constant, ε_{ecc} is the eccentricity of Earth's orbit, δ is the solar declination, φ is the location latitude, and ω_s is the half day length (time between sunrise and noon or noon and sunset) in radians. ε_{ecc} and ω_s are functions of the day in the year only, while δ also depends on the location longitude since its noon value is used, which yields more precise results. Details on calculating these parameters are included in Wald (2019).

The cloud-free atmospheric transmittance in Eq. (11) accounts for the transmittance of dry clean air (τ_0) and the transmittance due to absorption by aerosols (τ_a) and water vapor (τ_v), and it also incorporates a correction for elevation (c_{elev}):

$$\tau_{cf} = \left(\tau_0 \tau_a \tau_v\right)^{c_{elev}}. \tag{14}$$

To calculate τ_0, τ_a, τ_v, c_{elev}, D, and β, we follow Winslow et al. (2001). The transmittance of dry clean air is dependent only on the latitude (φ) and is calculated as follows:

$$\begin{aligned} &\tau_0 = 0.947 - \left(1.033 \times 10^{-5}\right)\left|\varphi\right|^{2.22} \qquad \text{for} \quad \left|\varphi\right| \le 80^\circ \\ &\tau_0 = 0.774 \qquad \text{for} \quad \left|\varphi\right| > 80^\circ. \end{aligned}, \tag{15}$$

The absorption by aerosols is extremely variable. Similar to Winslow et al. (2001), we set τ_a = 1 (i.e., no absorption).

The absorption by water vapor is calculated from the following:

https://doi.org/10.5194/gmd-2021-118
Preprint. Discussion started: 16 June 2021


Geoscientific Model Development Discussions

$$\tau_v = 0.9636 - 9.092 \times 10^{-5} \left(T_{mean} + 30\right)^{1.8232}, \quad (16)$$

where T_{mean} is the mean annual air temperature (°C). On wet days, when the daily precipitation is above 1 mm, τ_v is reduced by 0.13. The site elevation correction factor (c_{elev}) is calculated as follows:

$$c_{elev} = \left[1 - \left(2.2569 \times 10^{-5}\right) z_{\mathrm{ASL}}\right]^{5.2553}, \quad (17)$$

where z_{ASL} is the site elevation (m).

The factor D takes into account the error due to differences in day length:

$$D = \left[1 - \left(\omega_s - \pi/4\right)^2 / \left(2\omega_s\right)^2\right]^{-1}. \quad (18)$$

The factor β in Eq. (11) is mainly constant, except for regions with very large daily temperature ranges:

$$\beta = \max\left\{1.041, \quad 23.753 \Delta T_m / \left(T_{mean} + 273.16\right)\right\}, \quad (19)$$

where ΔT_m is the mean annual temperature range between the daily air temperature maximum and minimum.

Hourly shortwave radiation data were generated from the calculated daily solar irradiance by using the measured UVB radiation data as a weight function:

$$S_n(h) = UVB(h) \frac{S_{n\_day}}{UVB_{day}} = UVB(h) \frac{S_{n\_day}}{3600 \sum_{h=1}^{24} UVB(h)}, \quad (20)$$

where S_{n_day} and UVB_{day} are the daily values (J m^{-2} day^{-1}) and $S_n(h)$ and $UVB(h)$ are the mean values (W m^{-2}) for the h^{th} hour of the total and UVB solar radiation, respectively. When UVB radiation data are unavailable, the standard daily radiation profile can be used.

Unlike the other terms in Eq. (8), shortwave radiation is not completely absorbed in the lake surface layer but partially passes through the water. The shortwave radiation reaching a particular depth is calculated using the light extinction coefficient:

$$S_n(z) = S_n(0) \exp\left(-\lambda_e z\right), \quad (21)$$

where $S_n(z)$ and $S_n(0)$ are the shortwave radiations at water depth z and at the water surface, respectively, and λ_e is the light extinction coefficient calculated as suggested by Wu et al. (2020):

$$\lambda_e = 1.1925\, z^{-0.424}. \quad (22)$$

3.1.2. Longwave radiation

The net longwave radiation is the difference between the incoming downward atmospheric longwave radiation ($L_a^{\downarrow}$) and the outgoing upwards radiation from the lake surface ($L_s^{\uparrow}$). As direct measurement data of longwave radiation by pyrgeometers are not routinely available, longwave radiation may be calculated using the following formula:

$$L_n = \varepsilon L_a^{\downarrow} - L_s^{\uparrow} = \varepsilon\left[\varepsilon_a \sigma \left(T_a + 273.15\right)^4\right] - \varepsilon\sigma\left(T_s + 273.15\right)^4, \quad (23)$$

https://doi.org/10.5194/gmd-2021-118
Preprint. Discussion started: 16 June 2021


Geoscientific Model Development Discussions

where ε and ε_a are the emissivities of the lake surface and the atmosphere, respectively, T_s is the water surface temperature (°C), T_a is the air temperature at 2 m height (°C), and σ = 5.67x10^{-8} W m^{-2} K^{-4} is the Stefan-Boltzman constant. The emissivity of water is assumed to be 0.96 (e.g., Sun et al. 2007). The emissivity of the atmosphere depends on the water vapor and atmospheric temperature profile. Assuming a standard atmosphere, Brutsaert (1975) derived a formula for calculating the atmospheric emissivity under clear sky conditions:

$$\varepsilon_{ac} = 1.24\left[e_a/(T_a + 273.15)\right]^{1/7}, \tag{24}$$

where e_a is the water vapor pressure (hPa). Although other empirical formulas for calculating atmospheric emissivity are available, Brutsaert's (1975) expression (Eq. 24) was reported as the best in many studies of different climates (Wang and Dickinson, 2013). Because Eq. (24) refers to clear sky conditions, it is necessary to additionally account for cloud effects. Assuming that the emissivity of the water droplets in the clouds is approximately equal to one, Crawford and Duchon (1999) calculate the total atmospheric emissivity as follows:

$$\varepsilon_a = (1 - f)\varepsilon_{ac} + f \tag{25}$$

where f is the cloud cover, which ranges from 0 (clear sky) to 1 (total cloud coverage). This formula is considered the best formula in many studies (Wang and Dickinson, 2013). By substituting Eqs. (24) and (25) in Eq. (23), we obtain the expression for calculating the net longwave radiation:

$$L_n = \varepsilon\left\{\left[(1 - f)\varepsilon_{ac} + f\right]\sigma(T_a + 273.15)^4\right\} - \varepsilon\sigma(T_a + 273.15)^4. \tag{26}$$

As cloud fraction data are not available for the area of our study, climatological monthly values were used.

3.1.3. Latent and sensible heath flux

To calculate the latent and sensible heat flux, we use a slightly modified algorithm provided by Verburg and Antenucci (2010). Their code, which is publicly available at the National Institute of Water and Atmospheric Research (NIWA) website (NIWA, 2021), uses the bulk aerodynamic method based on the Monin-Obukhov similarity theory (Monin and Obukhov, 1954). According to this method, the sensible and latent heat fluxes can be calculated as follows:

$$H_s = \rho_a c_a C_H U_Z (T_s - T_a), \tag{27}$$

$$H_l = \rho_a L_v C_E U_Z (q_s - q_a), \tag{28}$$

where C_H and C_E are the transfer coefficients for sensible and latent heat flux, respectively, c_a = 1005 J kg^{-1} K^{-1} is the specific heat of air, $L_v \approx$ 2500 kJ kg^{-1} is the latent heat of evaporation, ρ_a is the air density (kg m^{-3}), and q_s and q_a are the specific humidities (kg kg^{-1}) at the water surface and measuring levels, respectively. Air density and specific humidity were determined from the ideal gas law equation and from the observed relative humidity, respectively.

The transfer coefficients were calculated in an iterative procedure, initially assuming neutral atmospheric conditions:

$$C_D = k^2/\left[\ln(h/z_0) - \psi_M\right]^2, \tag{29}$$

https://doi.org/10.5194/gmd-2021-118
Preprint. Discussion started: 16 June 2021

Geoscientific Model Development Discussions

$$C_E = k^2 / \{[\ln(h/z_0) - \psi_M][\ln(h/z_E) - \psi_E]\} = kC_D^{1/2} / [\ln(h/z_E) - \psi_E], \quad (30)$$

$$C_H = C_E, \quad (31)$$

where C_D is the drag coefficient, h is the height above ground (m), z_0 and z_E are the roughness lengths (m), and ψ_M and ψ_E are the stability functions for momentum and vapor, respectively. The stability functions are defined through the stability parameter $\zeta = h/L$, where L is the Monin-Obukhov length:

$$L = \frac{-\rho_a u_*^3 T_V}{kg\left(\frac{H_s}{c_a} + 0.61\frac{(T_a + 273.16)H_l}{L_v}\right)}, \quad (32)$$

where T_v is the virtual temperature. Obviously, L depends on H_s and H_l while H_s and H_l depend on the stability of the atmosphere. Therefore, to calculate H_s and H_l, an iterative procedure has to be used. The procedure is initiated by assuming neutral conditions ($\psi_M = \psi_E = 1$). Further details on the calculation of roughness lengths, stability functions and the iterative process itself can be found in Verburg and Antenucci (2010).

3.1.4. Heat brought by precipitation

Assuming the first lake layer in the numerical model is thick enough so that the precipitation amount is negligible compared to the surface layer water mass ($\Delta z_1 >> P\Delta t$), it is easy to come to the following equation for calculating the heat flux brought by precipitation:

$$H_p = Pc_p T_{prec} / (1000 \times 3600), \quad (33)$$

where P is the hourly precipitation (mm h^{-1}) and T_{prec} is the precipitation temperature (°C). Since T_{prec} was not available, the air temperature was used instead.

3.2. Convective mixing

During the night, the net heat flux at a lake surface is generally negative. Consequently, unstable lake stratification is established. However, this unstable stratification is short-lived because the higher density water forming on top of the lake quickly sinks and mixes with the lower density water below it, thus restoring equilibrium (i.e., minimum potential energy). As Sun et al. (2007) pointed to the importance of introducing a convective mixing mechanism in a water temperature model, we also incorporated this mechanism in the present model. Namely, after each time step of integration, the model algorithm checks whether the upper layer in each pair of two adjacent layers has a higher density than the lower layer. If this occurs, then the two layers are assumed to mix completely, which results in uniform temperature:

$$T_{j\_new} = T_{j+1\_new} = (T_j \Delta z_j + T_{j+1}\Delta z_{j+1}) / (\Delta z_j + \Delta z_{j+1}), \quad (34)$$

https://doi.org/10.5194/gmd-2021-118
Preprint. Discussion started: 16 June 2021

Geoscientific Model Development Discussions

where Δz_j and Δz_{j+1} represent the thickness of the j-th (upper) and (j+1)-th (lower) layers, respectively; T_j and T_{j+1} are the water temperatures in these layers before convective mixing, respectively, and T_{j_new} and T_{j+1_new} are the temperatures in these layers after convective mixing, respectively.

3.3. Model setup

The model code is written in MATLAB programming language. Equation (1) is discretized using the backward Euler scheme:

$$\frac{c_p \rho_j}{\Delta t}\left(T_j^{n+1} - T_j^n\right) = \frac{1}{\Delta z_j}\left[\left(k_m + k_{t,j+1/2}\right)\left(\frac{T_{j+1}^{n+1} - T_j^{n+1}}{z_{j+1} - z_j}\right) - \left(k_m + k_{t,j-1/2}\right)\left(\frac{T_j^{n+1} - T_{j-1}^{n+1}}{z_j - z_{j-1}}\right)\right] - \frac{1}{\Delta z_j}\left(\phi_{j+1/2}^n - \phi_{j-1/2}^n\right), \quad (35)$$

where the subscript denotes the layer or the boundary between two layers, and the superscript denotes the time increment. Notice that the convective term from Eq. (1) is omitted in Eq. (35) since the algorithm employs convective mixing in a separate procedure after the integration step only if density inversion is detected in the water column, as explained in chapter 3.2. Equation (35) can be rearranged as follows:

$$T_{j-1}^{n+1}\left(\frac{-k_m - k_{t,j-1/2}}{z_j - z_{j-1}}\right) + T_j^{n+1}\left(\frac{\Delta z_j c_p \rho_j}{\Delta t} + \frac{k_m + k_{t,j+1/2}}{z_{j+1} - z_j} + \frac{k_m + k_{t,j-1/2}}{z_j - z_{j-1}}\right) + T_{j+1}^{n+1}\left(\frac{-k_m - k_{t,j+1/2}}{z_{j+1} - z_j}\right) = \quad (36)$$
$$= \left(\frac{\Delta z_j c_p \rho_j}{\Delta t}\right) T_j^n + \left(\phi_{j+1/2}^n - \phi_{j-1/2}^n\right) \quad .$$

Equation (36) can be written in matrix form as follows:

$$\mathbf{M}\ \mathbf{T^{n+1}} = \mathbf{A}\ \mathbf{T^n} + \mathbf{B}\,. \quad (37)$$

Then, the solution for $\mathbf{T^{n+1}}$ is obtained as follows:

$$\mathbf{T^{n+1}} = \mathbf{M^{-1}A}\ \mathbf{T^n} + \mathbf{M^{-1}B}\,. \quad (38)$$

The implicit Euler scheme is unconditionally stable and thus does not have an upper limit for the time increment. Considering the time resolution of the available input data, the model was run with a time step of one hour. The vertical resolution in the model corresponds to the measuring depths and decreases with lake depth. The depths of the integration points were consistent with the sensors' depths, while the boundaries of the layers were set halfway between each pair of consecutive points (Fig. 4b). The layer thicknesses ranged from 0.35 m (surface layer) to 16 m (bottom layer). An overview of the model workflow is given in Fig. 4a.

A simulation was initiated in each hour of the periods in which both meteorological and water temperature observations were available. Each simulation was run for up to 30 days or until the end of the period with available data. Measured water temperature profiles were used for simulation initialization.

https://doi.org/10.5194/gmd-2021-118
Preprint. Discussion started: 16 June 2021

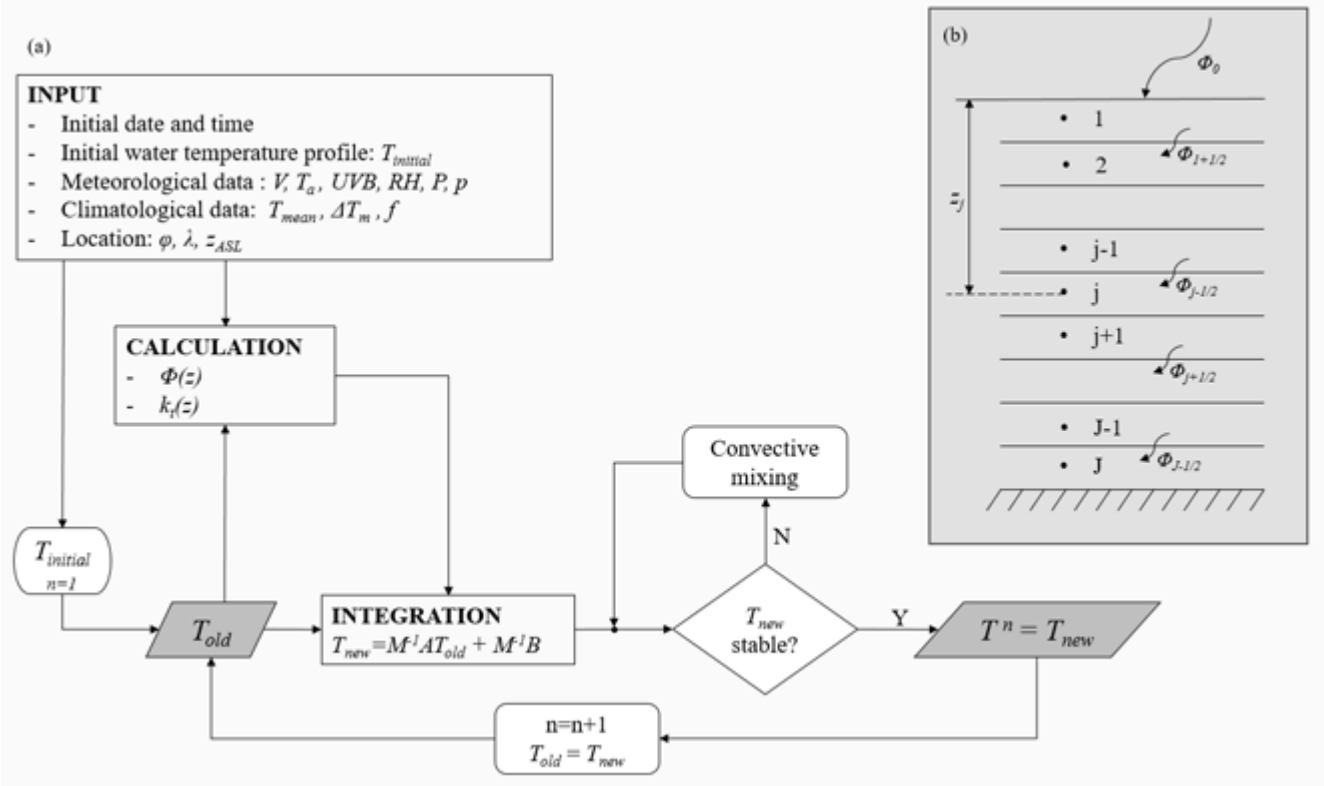

330 **Figure 4 Model configuration. Panel (a) shows a schematic overview of the model workflow. The input consists of the initial time and date, the initial water temperature profile $T_{initial}$, meteorological data (wind speed, air temperature, UVB radiation, relative humidity, precipitation, and atmospheric pressure), climatological data (mean annual air temperature, mean annual temperature range between the daily air temperature maximum and minimum, and mean monthly cloud cover), and location data (location latitude, longitude, and altitude above sea level). Panel (b) shows the layer setup. Points from 1 to J indicate the integration points**
335 **where water temperatures are calculated, and z_j is the depth of the j-th point. The horizontal lines indicate boundaries between layers, $\Phi_{j\pm1/2}$ are the heat fluxes across the layer boundaries, and Φ_0 is the net surface heat flux.**

4 Measures of the model performance

First, a sensitivity analysis was performed to assess the dependence of the model performance on the simulation length. Predicted water temperatures and vertical temperature gradients were compared with the corresponding observed values for
340 simulation lengths from 1 to 30 days. The model performance for each simulation length was evaluated by common bivariate measures. The mean bias error (MBE) is used to assess the tendency of the model to over- or underpredict the temperature. The mean absolute error (MAE) and the root mean square error (RMSE) both provide information about the error central tendency. However, RMSE also accounts for the distribution of the error and becomes larger as the error variability increases. RMSE places more weight on large errors, which makes it more sensitive to outliers. Due to all of the above, it has been argued
345 that MAE is a more natural measure of average error than RMSE (Willmott and Matsuura, 2005). The maximum absolute error (MaxAE) is not a measure of systematic error, but it was calculated as a measure showing the most extreme outlier. The above measures are calculated from the following expressions:

https://doi.org/10.5194/gmd-2021-118
Preprint. Discussion started: 16 June 2021

Geoscientific Model Development Discussions

$$\mathrm{MBE} = \frac{1}{n}\sum_i \left(P_i - O_i\right), \tag{39}$$

$$\mathrm{MAE} = \frac{1}{n}\sum_i \left(\left|P_i - O_i\right|\right), \tag{40}$$

$$\mathrm{RMSE} = \left[\frac{1}{n}\sum_i \left(P_i - O_i\right)^2\right]^{1/2}, \tag{41}$$

$$\mathrm{MaxAE} = \max\left\{\left|P_i - O_i\right|\right\}, \tag{42}$$

where O and P correspond to the observed and predicted values, respectively, while n is the number of corresponding pairs of these values.

The index of agreement values were calculated using three different formulas proposed by Willmott et al. (2012), namely, the original ($\mathrm{IA_{orig}}$), modified ($\mathrm{IA_{mod}}$) and refined ($\mathrm{IA_{ref}}$) index of agreement:

$$\mathrm{IA_{orig}} = 1 - \frac{\sum_i \left[\left(P_i - \overline{O}\right) - \left(O_i - \overline{O}\right)\right]^2}{\sum_i \left(\left|P_i - \overline{O}\right| + \left|O_i - \overline{O}\right|\right)^2} = 1 - \frac{\sum_i \left(P_i - O_i\right)^2}{\sum_i \left(\left|P_i - \overline{O}\right| + \left|O_i - \overline{O}\right|\right)^2}, \tag{43}$$

$$\mathrm{IA_{mod}} = 1 - \frac{\sum_i \left|P_i - O_i\right|}{\sum_i \left(\left|P_i - \overline{O}\right| + \left|O_i - \overline{O}\right|\right)}, \tag{44}$$

$$\mathrm{IA_{ref}} = 1 - \frac{\sum_i \left|P_i - O_i\right|}{2\sum_i \left|O_i - \overline{O}\right|} \quad \text{for} \quad \sum_i \left|P_i - O_i\right| < 2\sum_i \left|O_i - \overline{O}\right|, \tag{45a}$$

$$\mathrm{IA_{ref}} = \frac{2\sum_i \left|O_i - \overline{O}\right|}{\sum_i \left|P_i - O_i\right|} - 1 \quad \text{for} \quad \sum_i \left|P_i - O_i\right| > 2\sum_i \left|O_i - \overline{O}\right|. \tag{45b}$$

The IA represents a measure of the relative covariability of the observed and predicted values with respect to the observed mean. The original IA (Eq. (43)) uses the square of the difference between predicted and observed values, which is why it overestimates the influence of large errors, similar to the RMSE, which is why the square is replaced with an absolute value in the modified version (Eq. (44)); thus, $\mathrm{IA_{mod}}$ is less sensitive to outliers than $\mathrm{IA_{orig}}$. $\mathrm{IA_{mod}}$ approaches 1 (perfect agreement) more slowly than $\mathrm{IA_{orig}}$, which means that $\mathrm{IA_{mod}}$ is more conservative and allows for finer comparisons of different models with relatively good performance. In $\mathrm{IA_{ref}}$ (Eq. (45)), the prediction variability in the denominator is replaced with the

https://doi.org/10.5194/gmd-2021-118
Preprint. Discussion started: 16 June 2021


Geoscientific Model Development Discussions

observation variability. IA_{orig} and IA_{mod} range from 0 to 1, where a value of 0 means that the prediction and observation variabilities are totally out of phase, while a value of 1 means perfect fit. IA_{ref} ranges from -1 to 1 and has a well-defined lower boundary (Eq. (45b)), which allows for a better comparison of models with poor performance. However, it should be stressed that IA_{ref} approaching the value of -1 does not necessarily indicate poor model performance because it can also be a result of low observation variability.

The second goal of this study was to examine the ability of the model to predict the springtime onset of lake stratification assuming that there are no measured water temperature data available. For this purpose, a simulation initiated with approximately constant water temperature throughout the entire lake column (≈ 4 °C), which is characteristic of the period when a lake is mixed, was run for the entire year, starting from 1 January 2019. Although accurate results were not expected for the yearlong simulation, the goal of this analysis was to evaluate the extent to which the model can provide relevant information regarding the stratification/thermocline depth. Such an approach is particularly appealing for lakes that are completely mixed during the winter since it does not require measurement of the water temperature profile to initiate the simulation.

5 Results and discussion

Based on sporadic observations of the vertical temperature profiles in the Plitvice Lakes, previous studies suggest that Lake 1 and Lake 12 are dimictic (Klaić et al., 2018). Dimictic lakes are covered by ice during winter; they mix in spring and fall; and they are stratified in summer. The continuous observation data of the vertical temperature profiles in Lake 1 and Lake 12 shown in Fig. 2a and c, for the first time clearly illustrate that during the field campaign, both lakes behaved as warm monomictic lakes. Specifically, they were mixed during winter but stratified at other times. Furthermore, monomictic lakes (which are frequently found in temperate and tropical latitudes) typically do not freeze, and the two studied lakes did not freeze during the entire field campaign since the wintertime temperatures in the top lake layers were above 0 °C (Fig. 2b and d).

As the main driver of the lake temperature profile is the surface heat flux, it is interesting to first analyze its terms. Figure 5 shows the modeled mean diurnal variation in the total heat flux and the heat flux terms for a typical winter (a) and summer month (b). The solar heat flux is an order of magnitude higher than the other components of the total heat flux, which indicates that it is one of the main factors affecting the lake water temperature. Next in magnitude is the net longwave radiation, followed by the latent heat flux. The last two components are negative and are responsible for the negative heat flux, or cooling, at night.

The observed and predicted water temperatures for various simulation lengths for 2019 are shown in Fig. 6. (Lake 1, note that lake temperature measurements started in July) and Fig. 7 (Lake 12). The model performed reasonably well. Namely, the onset of the stratification period (Fig. 7) and both the vertical temperature profile and deepening of the thermocline over time were well captured (Figs. 6 and 7). Simulation results for Lake 12 reproduce the observed data more closely, while for Lake 1 higher discrepancies between simulated and observed data are present, especially for simulation lengths of 5 days and above.

https://doi.org/10.5194/gmd-2021-118
Preprint. Discussion started: 16 June 2021

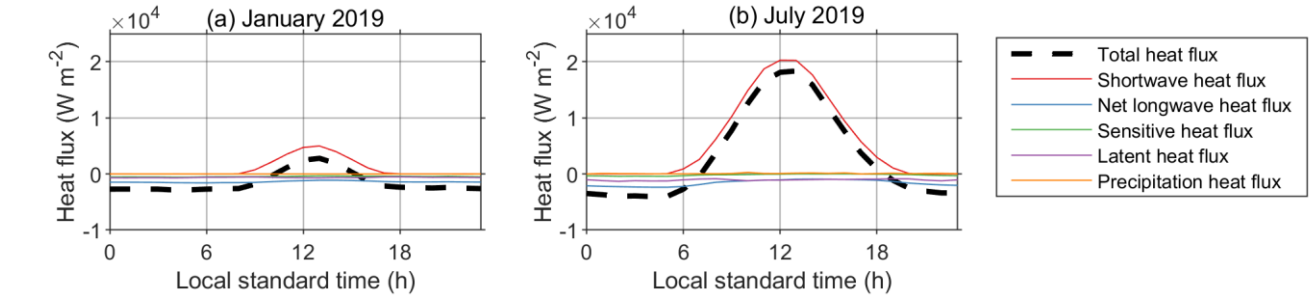

Figure 5 Modeled mean diurnal variations in the heat flux at the surface of Lake 12 for January (a) and July 2019 (b).

Figure 8 shows a closer view of the observed vs. predicted temperatures at depths of 0.2 m, 5 m, 15 m and 27 m for the period between 6 July 2019 and 31 December 2019. This period was chosen because it is the longest period in which all necessary data (both meteorological and water temperatures for both lakes) were available. Additionally, observed vs. predicted temperature gradients and the prediction errors for both temperature profiles and temperature gradients for the same sample period are presented in Appendix A. As expected, the departure of the predicted from the observed quantities increases with the length of the simulation period. However, even the longest simulation runs (30 days) produced qualitatively acceptable results. Departures of the predicted hourly mean temperatures were mainly $\leq \pm 2$°C and $\leq \pm 1$°C for Lake 1 and Lake 12, respectively, except near the surface where they were mainly $\leq \pm 4$C and $\leq \pm 2.5$°C for Lake 1 and Lake 12, respectively. The temporal temperature variations at various depths were satisfactorily simulated (Figs. 8, A1 and A2). Furthermore, thermocline depths and their deepening in time were well captured by the model (Figs. A3 and A5). However, the results also suggest that the lake temperatures in the epilimnion and hypolimnion are somewhat over- and underpredicted, respectively (Figs. 8, A1 and A2).

Although the model satisfactorily reproduced the temporal variations in the lake temperatures at the hourly scale, it was not able to reproduce the internal seiches that were previously documented for both lakes (Klaić et al., 2020a, 2020b). This finding is not surprising since the present model is based solely on the energy-budget approach; thus, except for vertical mixing of the two adjacent layers under unstable stratification, it does not account for any hydrodynamic behavior.

Figures 9 and 10 show the calculated model performance measures for both lakes. The model overestimates the water temperature in the epilimnion, especially near the surface, with an MBE from 1.3 °C and 0.8 °C for 1-day simulations, up to 4.2 °C and 2.9 °C for 30-day simulations, in Lake 1 and Lake 12, respectively (Figs. 9a and 10a). The MAE near the surface in Lake 1 starts from 1.3 °C for 1-day simulations and increases relatively steadily to 4.2 °C for 30-day simulations (Figs. 9b). In Lake 12, however, it starts from 0.9 °C for 1-day simulations and reaches a value of approximately 2.5 °C for a simulation length of 15 days and slowly increases to 2.9 °C as the simulation length reaches 30 days (Fig. 10b).

https://doi.org/10.5194/gmd-2021-118
Preprint. Discussion started: 16 June 2021

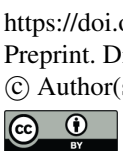

Geoscientific Model Development
Discussions
Open Access
EGU

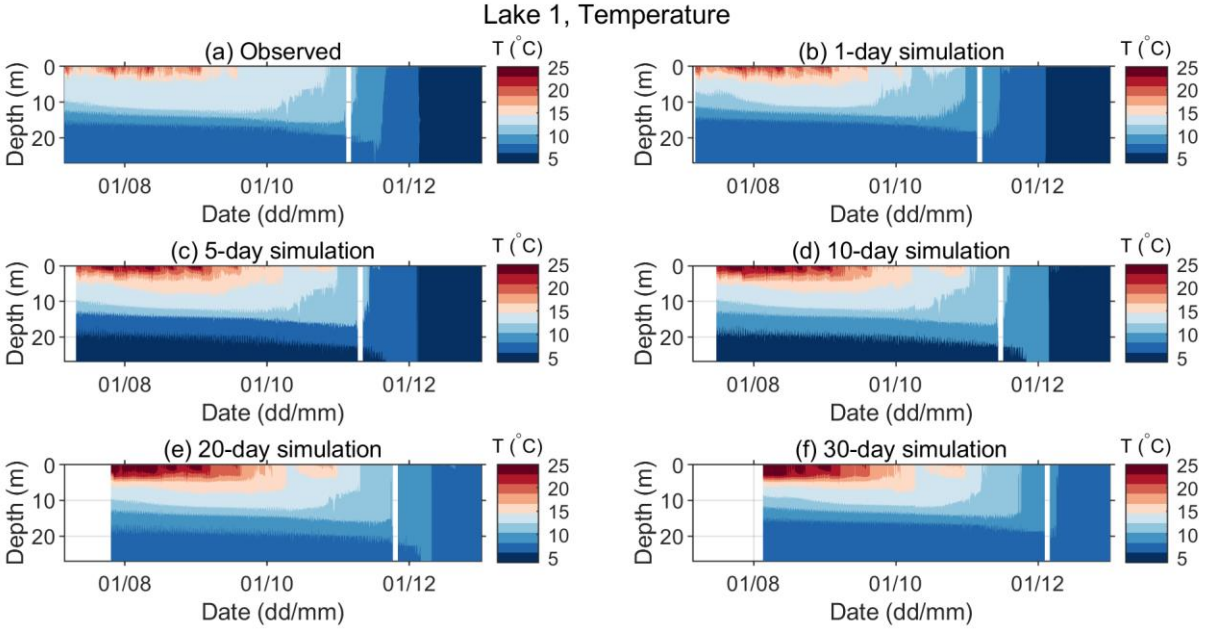

Figure 6 Observed (a) and predicted (b-f) water temperatures of Lake 1 for different simulation lengths in the period between 06 July 2019 and 04 November 2019. Periods with missing data are seen as white vertical stripes.

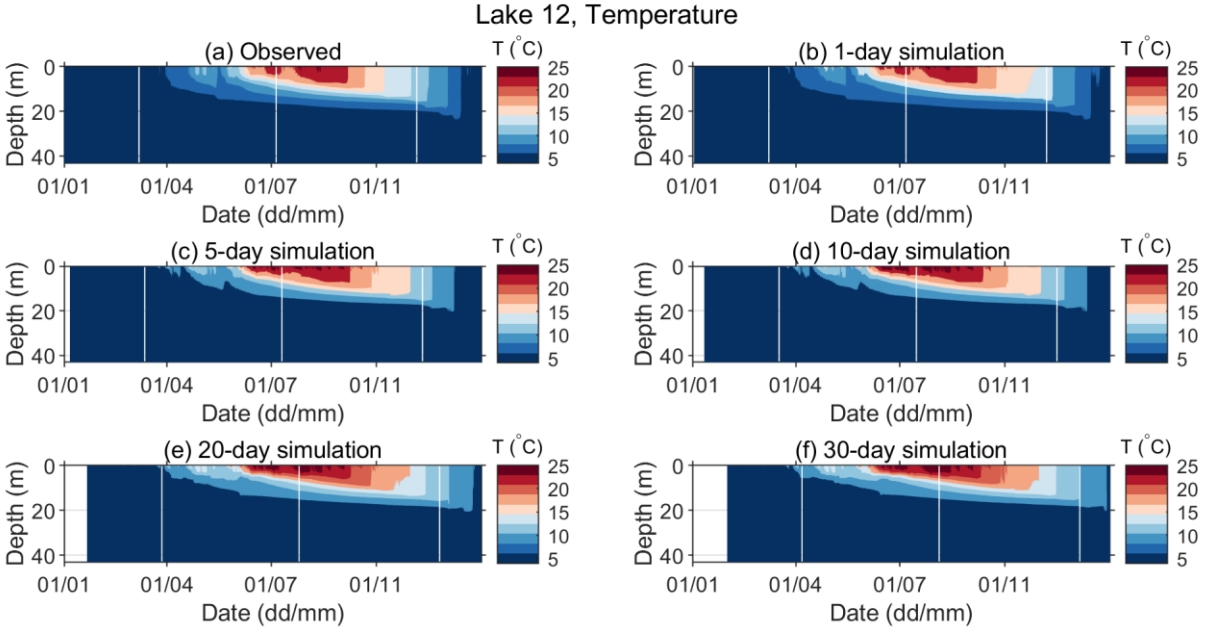

425 **Figure 7 Observed (a) and predicted (b-f) water temperatures of Lake 12 for different simulation lengths for 2019. Periods with missing data are seen as white vertical stripes.**

https://doi.org/10.5194/gmd-2021-118
Preprint. Discussion started: 16 June 2021

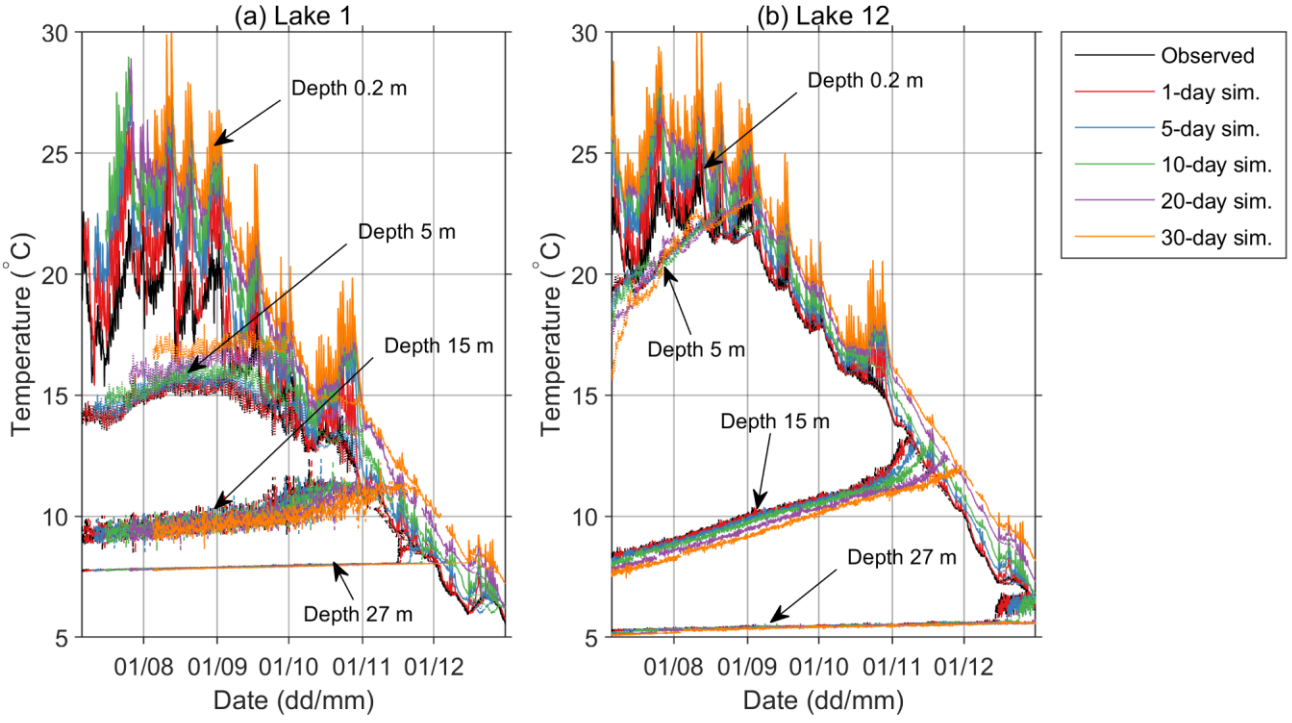

Figure 8 Observed and predicted water temperatures at depths of 0.2 m, 5 m, 15 m and 27 m for different simulation lengths in (a) Lake 1 and (b) Lake 12

Couple of factors could lead to overestimated temperatures in the upper lake layers. The first is the underestimation of turbulent mixing and turbulent heat transfer, especially in periods of high winds. As seen from Figs. A1 and A2, this overestimation of the uppermost part of the lake is more pronounced for Lake 1 than for Lake 12. As argued in Section 2.2.2, measuring site M (where the data used for the atmospheric forcing of the model are measured) is more representative for Lake 1 than for Lake 12. Accordingly, due to its higher altitude and less sheltered position, Lake 1 is more likely exposed to winds stronger than those measured at site M, and thus, both the turbulent mixing and the consequent heat transfer are likely to be stronger than modeled.

The second possible reason is the overestimation of the shortwave radiation extinction coefficient. This coefficient depends on the amount of dissolved organics and particulates in the lake water and can thus be calibrated to reproduce the lake physical properties more closely. We did not proceed with extinction coefficient calibration because our goal was to investigate the model performance and its general applicability without location-specific fitting.

Finally, it is possible that the surface heat flux has been overestimated, as the simplified approach used for its calculation is characterized by limited reliability.

https://doi.org/10.5194/gmd-2021-118
Preprint. Discussion started: 16 June 2021

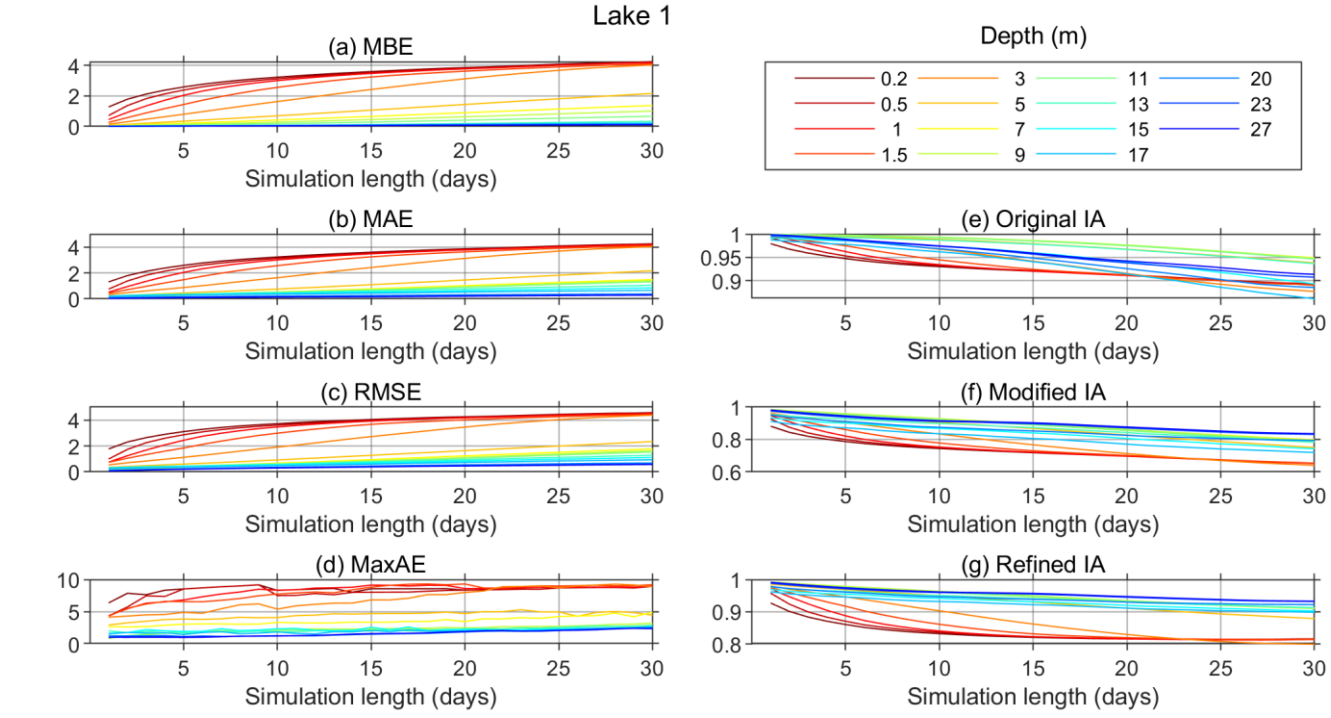

Figure 9 Model performance parameters for Lake 1.

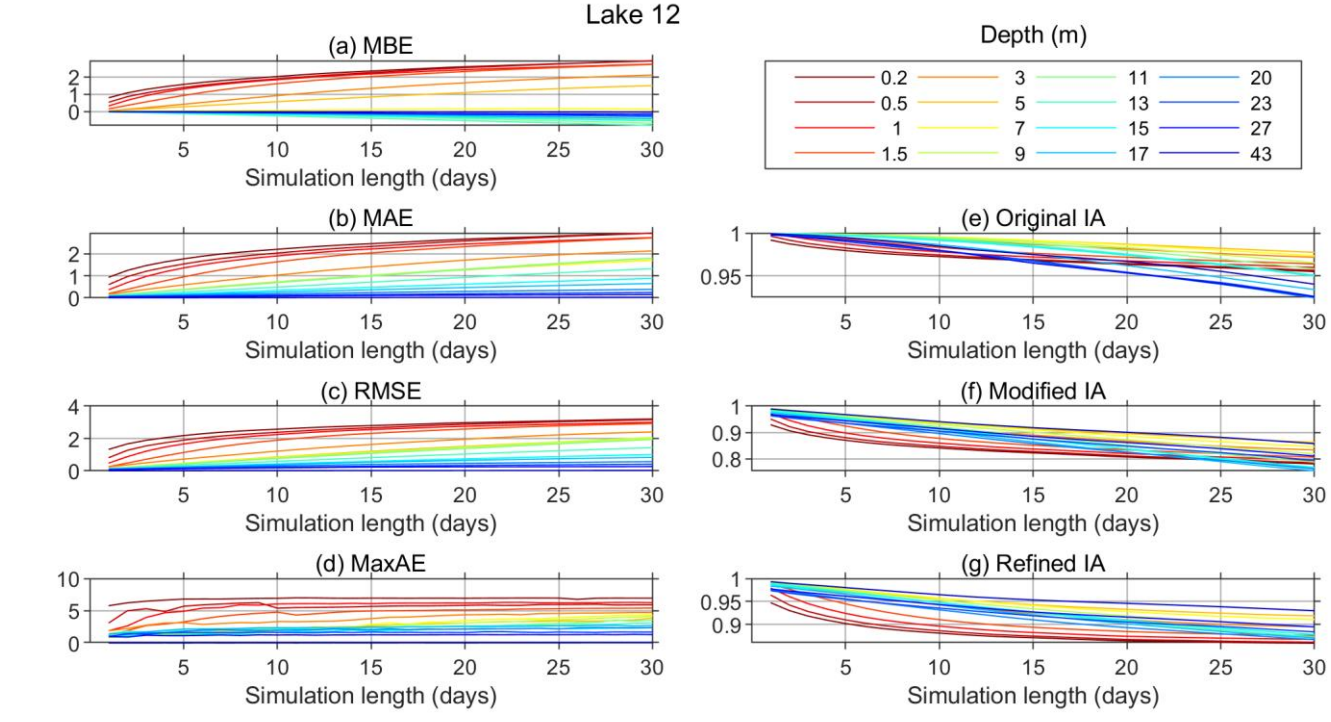

Figure 10 Model performance parameters for Lake 12.

https://doi.org/10.5194/gmd-2021-118
Preprint. Discussion started: 16 June 2021


Geoscientific Model Development Discussions

In the hypolimnion, the values of the MBE, MAE, RMSE, and MaxAE remain particularly low, especially for the deepest layers, for both lakes regardless of the simulation length (Figs. 9 and 10). These low values are a result of the low temperature variability in the deep lake layers, which is not taken into account in the formulation of these measures. In Lake 12 the MBE in the hypolimnion is slightly negative and reaches a value of -0.8 °C, while in Lake 1 the MBE stays positive throughout the lake depth and is close to zero in the hypolimnion. On the other hand, regardless of the formulation (original, modified or reference), the IA takes the temperature variability into account and therefore decreases with the increase of the simulation length even in the deep layers, indicating poorer performance as the simulations get longer.

Further inspection of the results for temperature and temperature gradients in Lake 12 (Figs. A2 and A6) shows that the temperature prediction in the metalimnetic layer (thermocline region) where the temperature gradients were the highest, was rather challenging. The model performed relatively poorly in this region, which is particularly noticeable for longer simulation periods.

As seen from Figs. 9 and 10, MaxAE did not increase significantly with increasing simulation length for either of the two lakes. As expected, MaxAE was highest near the surface and the maximum values for both lakes were relatively high (9.2 °C at 1 m depth and 7 °C in the surface layer for Lake 1 and Lake 12, respectively).

Figure 11 shows the monthly means of the observed and modeled vertical temperature profiles for Lake 12. The results for Lake 1 are not shown because the necessary observation data were not available throughout any complete year during the observational campaign. The model successfully reproduced the annual variation in the temperature profile throughout 2019, including the stratification onset and its termination and the thermocline deepening over time. As the heating starts in spring and continues through summer, the model tends to overpredict the temperatures in the uppermost part of the lake and underpredict the temperatures in the thermocline region (Fig. 11c–h). The difference between the predicted and observed surface temperature in the summer months reaches approximately 4 °C for the longest simulation period. This finding is consistent with the above presented discussion of the model performance measures. In August (Fig. 11h), although the stratification was still strong, the effects of convective mixing during the night started to affect the monthly mean. In the following months (Fig. 11i–l), the mixing depth grew and reached a maximum depth of approximately 20 m in December (Fig. 11l), while the lake stratification was much weaker than that in previous months. In these months of significant convective overturn, the deviation of the predicted from the observed epilimnion temperature is also observed. It becomes more significant with simulation length and reaches approximately 2 °C for the longest simulation period.

The second goal of this study was to examine the ability of the model to predict the onset and termination of stratification and the deepening of the thermocline by yearlong simulation. Because all necessary data for the entire year were only available for 2019, the first day of the yearlong simulation was set to 1 January 2019. For Lake 12, the simulation was initiated with a nearly constant water temperature profile (≈ 4 °C) that was observed for 1 January because these data were available, although a constant temperature of ≈ 4 °C that was generally observed over the entire water column (which is typical for the wintertime period when a lake is mixed) can be used instead.

https://doi.org/10.5194/gmd-2021-118
Preprint. Discussion started: 16 June 2021

Geoscientific Model Development Discussions
Open Access
EGU

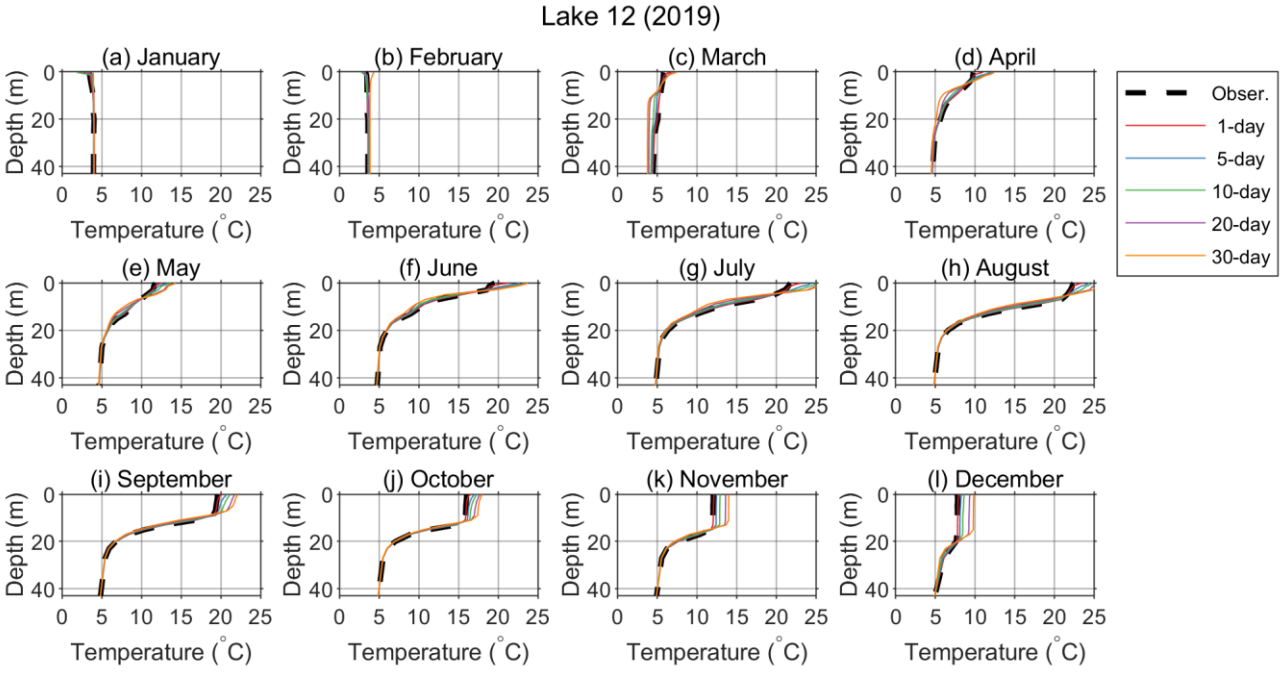

Figure 11 Annual variation in the vertical profile of the water temperature. Panels (a) to (l) show the monthly means of the observed and predicted values in Lake 12 for 2019.

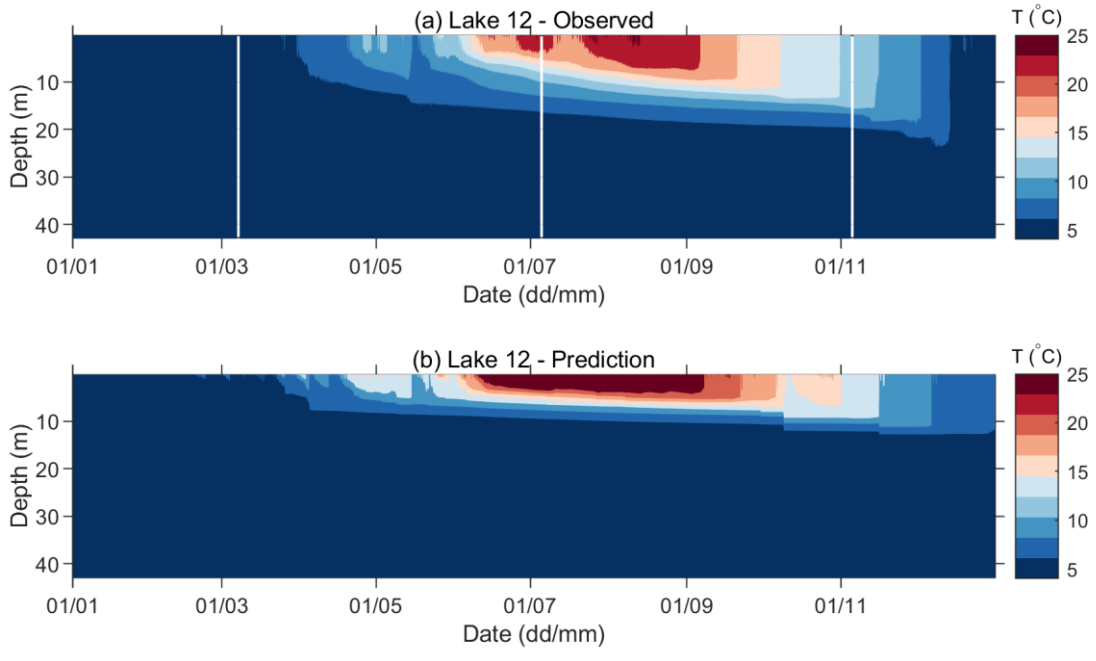

Figure 12 Observed (a) and predicted (b) water temperature for Lake 12 in 2019. The predicted temperature is obtained by a single yearlong simulation run initiated on 1 January 2019.

https://doi.org/10.5194/gmd-2021-118
Preprint. Discussion started: 16 June 2021

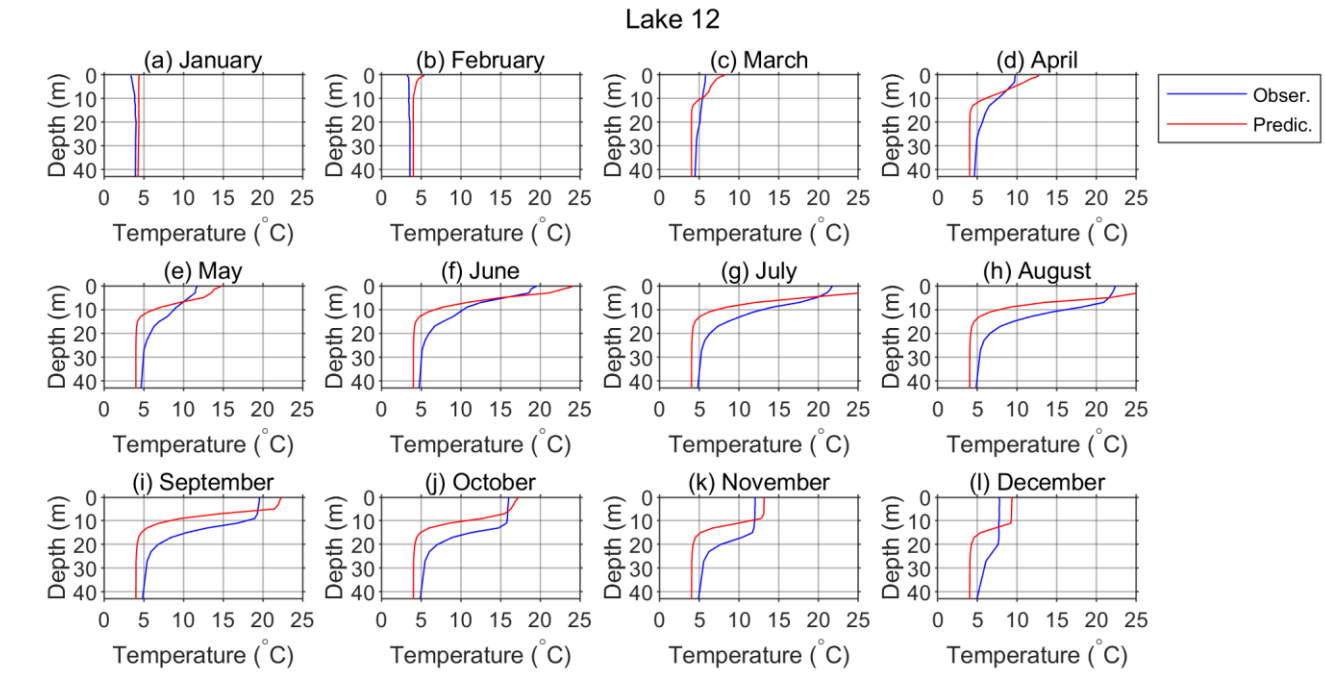

Figure 13 Monthly means of the observed (blue) and predicted (red) water temperature vertical profiles for Lake 12 in 2019. Predicted temperatures are obtained by a single yearlong simulation run initiated on 1 January 2019.

Figure 12 shows the contour diagrams of the observed and predicted water temperatures for Lake 12. Such results for Lake 1 are not shown because they were almost identical to those obtained for Lake 12. Namely, meteorological forcing drove temperature changes. If the same forcing was used for both lakes, then the only other factor that can introduce a difference in the results was the initial vertical profile, which was very similar for both lakes. As previously pointed out in the discussion of model performance, the model generally overpredicted the temperatures of the upper layers and underpredicted them for the lower layers. Consequently, the thermocline depth was underpredicted by approximately half and the simulated thermocline deepening was weaker than the observed thermocline depth. However, the onset and termination of the stratification period were well predicted, with the onset being captured somewhat better than the termination.

The observed and modeled monthly profiles that were obtained by the yearlong simulation are shown in Fig. 13. Here, the model generally underpredicted both the monthly mean lake temperatures (except near the surface) and thermocline depth, where discrepancies between the modeled and observed profiles were largest in the thermocline region. Nevertheless, the modeled results still qualitatively reproduced monthly mean profiles and their annual variation. It is also noted that the discrepancy between the observed and modeled temperatures in the thermocline region increased as stratification strengthened and then decreased as stratification weakened in late fall.

The comparison of model performance with other models is not strait forward because few studies systematically report statistical performance measures, the calculation methods are not always clearly stated, and there is no consensus on which measures are to be reported. No performance measure data referring to certain simulation lengths were found; however, few

https://doi.org/10.5194/gmd-2021-118
Preprint. Discussion started: 16 June 2021


Geoscientific Model Development Discussions

studies reported on single longer simulations. These results are summarized in Table 2. For a yearlong simulation of the water temperature in a small dimictic lake, Martynov et al. (2010) reported a surface temperature RMSE of 1.8 °C for an eddy diffusivity model (Hostetler model) and 3.2 °C for a two-layer model (FLake). Bruce et al. (2018) ran a two-year simulation for 32 different lakes using the GLM model, and the calculated RMSEs for the entire vertical profile, epilimnion, and hypolimnion were 1.34, 1.62, and 1.31 °C, respectively. MacKay (2012) ran a bulk mixed model simulation for approximately a month and a half and reported a surface temperature MBE < 1 °C.

The yearlong simulation in this study resulted in a surface temperature RMSE of 2.3 °C; in the hypolimnion, the RMSE was lower in the deepest layer at 0.7 °C, but for the depth of 23 m, it was 1.6 °C. The RMSE was the highest in the thermocline region, where it reached a maximum of 5 °C. The RMSE for the entire profile was 3.1 °C. The surface temperature MBE was 2.4 °C. The maximum MBE was again in the thermocline region and equaled -3.7 °C. This systematic underprediction in the thermocline region can also be noticed in Fig. 13. Considering the lake surface, entire vertical profile, epilimnion and hypolimnion temperature, the model performance for the yearlong simulation was satisfactorily since it was comparable with the performances of other models (Table 2), while for the thermocline region, it was poor.

Table 2 Comparison of the present model performance with other models.

Reference	Model	Application area	Simulation length	RMSE	MBE
	Present model	small monomictic lake	1 year	3.1°C (entire vertical profile) 2.3 °C (surface temp.) 0.7-1.6 °C (hypolimnion temp.)	2.4 °C (surface temp.)
	Present model	small monomictic lake	1.5 months		1.1 °C (surface temp.)
Martynov et al., 2010	Hostetler model	small dimictic lake	1 year	1.8 °C (surface temp.)	
Martynov et al., 2010	FLake model	small dimictic lake	1 year	3.2 °C (surface temp.)	
Bruce et. al, 2018	GLM model	32 different lakes		1.34 °C (entire vertical profile) 1.62 °C (epilimnion temp.) 1.31 °C (hypolimnion temp.)	
MacKay (2012)	Bulk mixed model	arctic lake	1.5 months		< 1 °C (surface temp.)

Finally, simulation results obtained for the model with and without turbulent thermal diffusion were compared. For both lakes, the results showed that the inclusion of this term did not result in noticeable model improvement (not shown here). This is in accordance with the suggestion of Sun et al. (2007) for shallow lakes.

https://doi.org/10.5194/gmd-2021-118
Preprint. Discussion started: 16 June 2021


Geoscientific Model Development Discussions

6 Summary and conclusions

The aim of this study was to offer a simple 1-D energy-budget model for the prediction of the vertical temperature profile in a small (less than 50 m deep) warm monomictic lake that is forced by a reduced number of input meteorological variables. Specifically, these include meteorological variables that are routinely measured at meteorological stations (i.e., the air temperature, relative humidity, atmospheric pressure, wind speed and precipitation) and UVB radiation data and climatological monthly means of cloudiness. In addition, an observed vertical profile of the lake temperature was used as an initial condition. The main challenge was to calculate the net heat flux on the lake surface and determine its components (i.e., the shortwave and longwave radiation, sensible and latent heat flux, and precipitation heat flux) from the available data. The model performance was evaluated using lake temperatures measured continuously during an observational campaign in two lakes of Plitvice Lakes, Croatia: Lake 1 (Prošće Lake) and Lake 12 (Kozjak Lake). The necessary meteorological data were provided by a single meteorological station located approximately 2 and 1.6 km from the lake temperature measuring points for Lake 1 and Lake 12, respectively. Except being further away from the meteorological station, Lake 1 has an approximately 100 m higher altitude than Lake 12, is surrounded by more complex orography and is very likely exposed to stronger winds and lower air temperatures than those used as meteorological input data. Accordingly, the model performance was somewhat poorer for Lake 1, which indicates the importance of the microlocation-specific input meteorological data, as the meteorological forcing is the main driver of the temperature profile evolution. In addition, the influence of the tributary water that inflows into Lake 1, which was not taken into account in the present model, could also contribute to higher differences between the modeled and measured temperatures in comparison to Lake 12.

Generally, the model overestimated temperatures in the epilimnion and underestimated them in the metalimnion while the position of the thermocline and its deepening are well captured. There are several possible causes of departures of modeled from measured temperatures. One of them is the underestimation of the turbulent heat transfer in the epilimnion, especially in periods of high winds. In addition, the model cannot simulate internal seiches and possible water exchange between the warmer epilimnion and colder hypolimnion. Other probable causes are the use of an inappropriate light extinction coefficient value and the limited reliability of the surface heat flux. Finally, better results are expected if cloud cover data with at least daily resolution are used instead of climatological monthly averages. However, considering all model simplifications, we conclude that the model performed reasonably well.

The sensitivity analysis of the model performance to the simulation length showed that when using appropriate meteorological forcing (as is the case of Lake 12), the model performance, especially in the epilimnion, steadily deteriorated up to a simulation length of approximately 15 days; however, a further increase in the simulation length up to 30 days had little effect on the model performance parameters.

Despite the model's shortcomings, the yearlong simulation showed that the model is able to predict the onset of stratification and convective overturn relatively precisely; however, it underestimated the thermocline depth and overestimated the epilimnion temperatures, which was similar to the results for the shorter interval simulations. Nevertheless, the values of the

https://doi.org/10.5194/gmd-2021-118
Preprint. Discussion started: 16 June 2021

model performance measures were comparable to those reported for other models. Thus, for a certain lake with no water temperature measurement data available, a yearlong simulation such as this would provide an assessment of lake stratification establishment, which can be useful for various studies dealing with lake biology, geochemistry, sedimentology, etc.

Our findings show that the inclusion of a turbulent thermal diffusion term in the lake model did not result in substantially better results for either lake with a medium depth (i.e., ≈ 37 and 46 m).

To further corroborate the general applicability of the present model, it should be applied to a larger number of different monomictic lakes. Nevertheless, in the present study, no lake-specific parameter tuning was performed. Thus, we expect similar model performance for other lakes if adequate meteorological forcing is employed.

https://doi.org/10.5194/gmd-2021-118
Preprint. Discussion started: 16 June 2021

Geoscientific Model Development Discussions

Appendix A

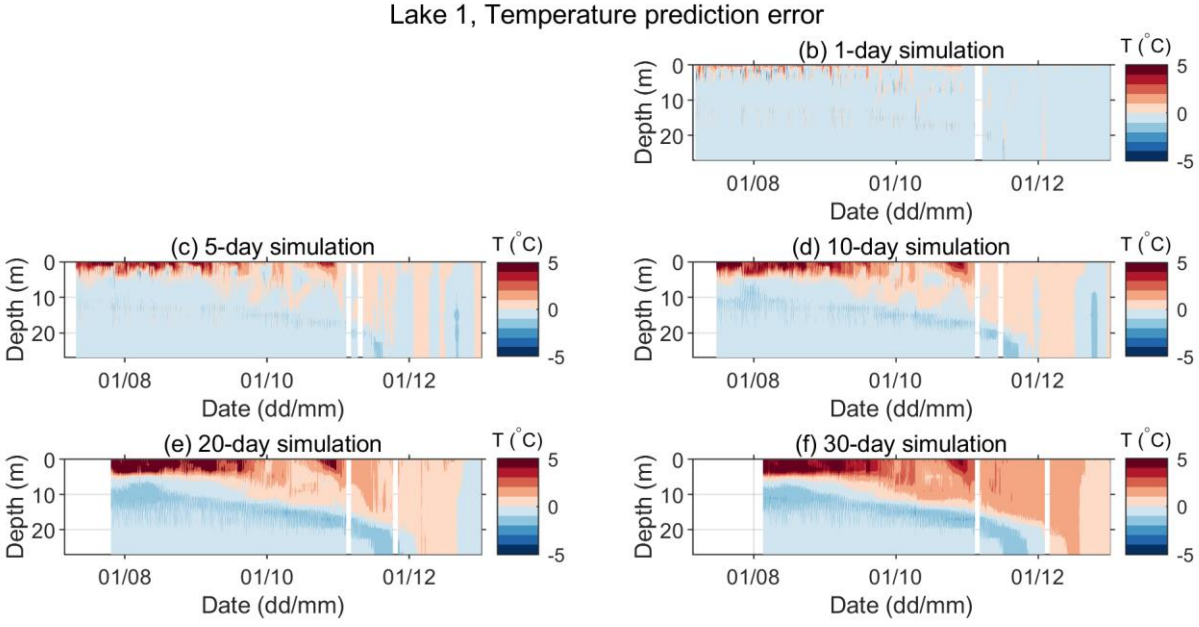

Figure A1 Error in the predicted water temperature (P_i-O_i) for Lake 1 for different simulation lengths for the period between 06 July 2019 and 04 November 2019. Panel (a) is omitted so that the panels' positions for different simulation lengths correspond to those in Fig. 6.

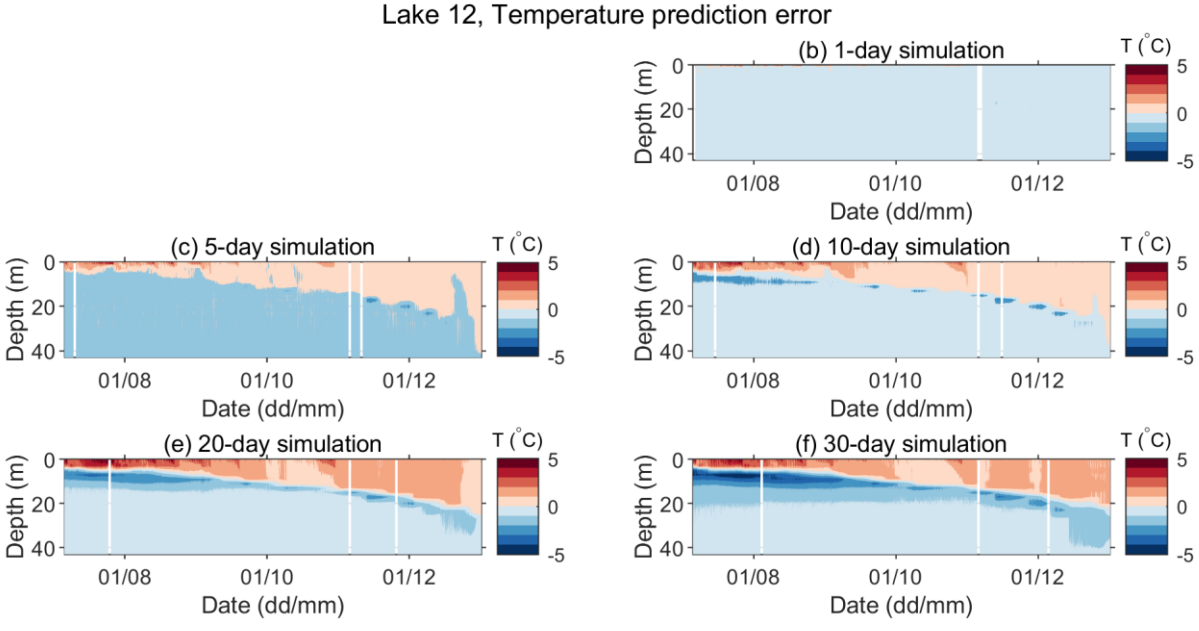

Figure A2 Error in the predicted water temperature (P_i-O_i) for Lake 12 for different simulation lengths in the period between 06 July 2019 and 04 November 2019. Panel (a) is omitted so that the panels' positions for different simulation lengths correspond to those in Fig. 7.

https://doi.org/10.5194/gmd-2021-118
Preprint. Discussion started: 16 June 2021

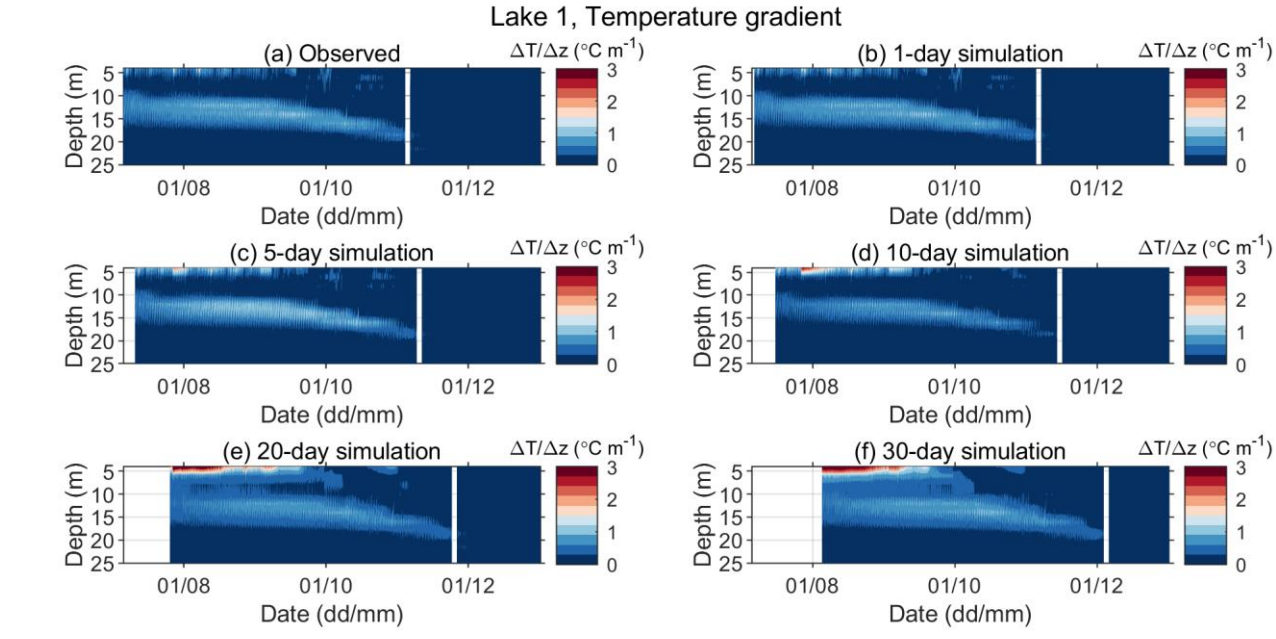

Figure A3 Observed (a) and predicted (b-f) vertical gradients of water temperature for Lake 12 for different simulation lengths in the period between 06 July 2019 and 04 November 2019.

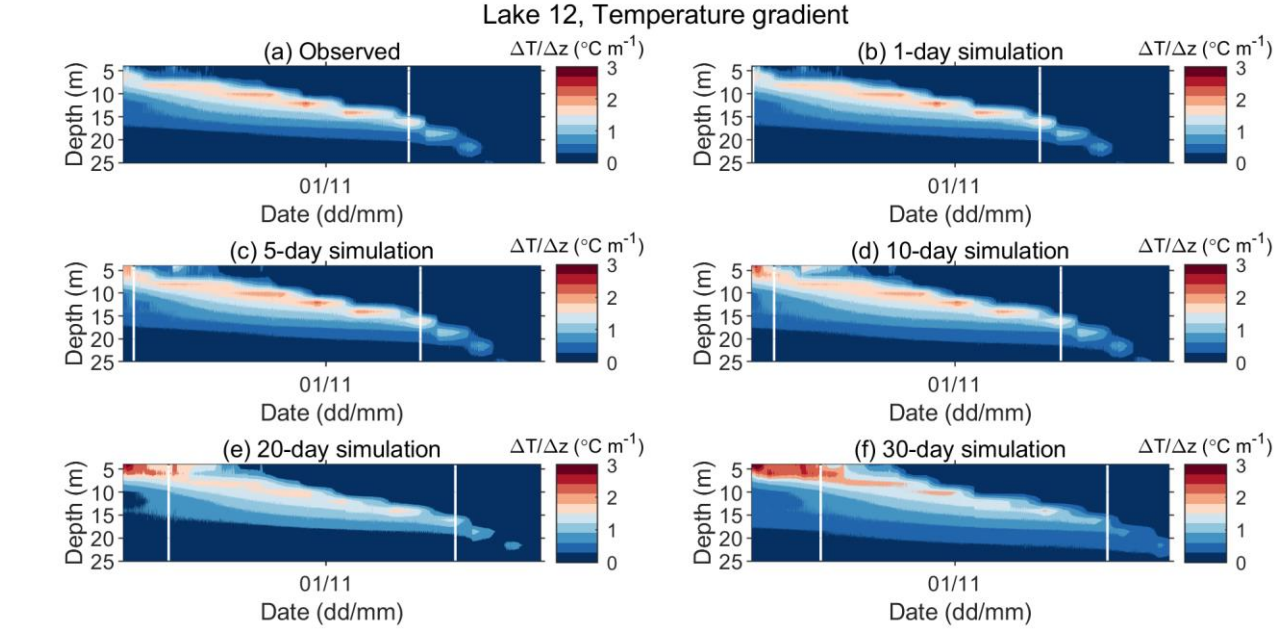

Figure A4 Error in the predicted vertical gradient of water temperature (P_i-O_i) in Lake 12 for different simulation lengths in the period between 06 July 2019 and 04 November 2019. Panel (a) is omitted so that the panels' positions for different simulation lengths correspond to those in Fig. 3.

https://doi.org/10.5194/gmd-2021-118
Preprint. Discussion started: 16 June 2021

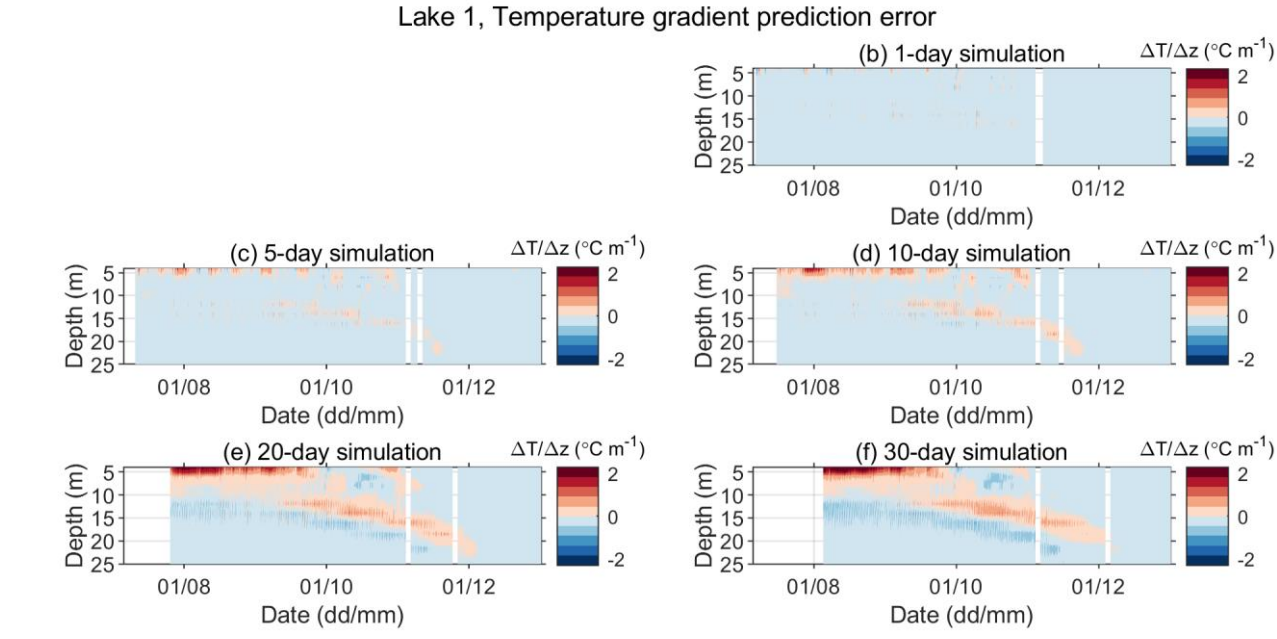

Figure A5 Observed (a) and predicted (b-f) vertical gradients of water temperature in Lake 1 for different simulation lengths in the period between 06 July 2019 and 04 November 2019.

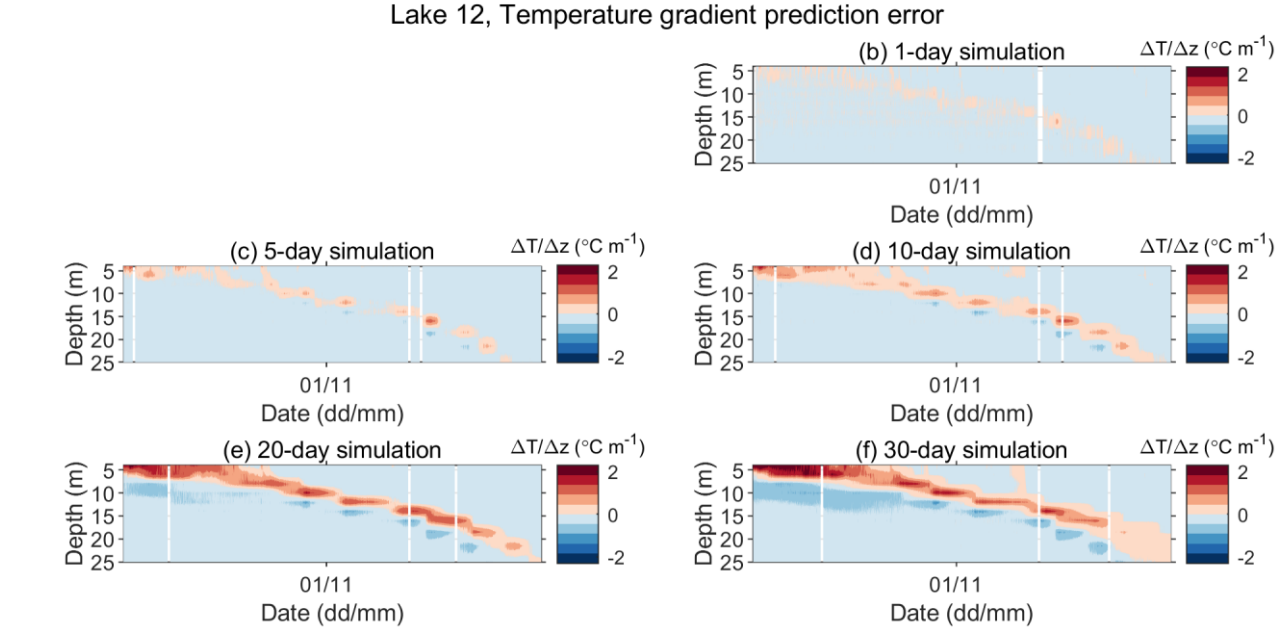

Figure A6 Error in the predicted vertical gradient of water temperature (P_i-O_i) in Lake 12 for different simulation lengths in the period between 06 July 2019 and 04 November 2019. Panel (a) is omitted so that the panels' positions for different simulation lengths correspond to those in Fig. 5.

https://doi.org/10.5194/gmd-2021-118
Preprint. Discussion started: 16 June 2021

Code and data availability

The SIMO v1.0 code is published under Creative Commons Attribution 4.0 International license and it is available at https://zenodo.org/record/4679796#.YHN41ugzaYE (last access: 11 April 2021), doi: 10.5281/zenodo.4679796.
Lake water temperature data are available on request for research purposes by contacting Zvjezdana B. Klaić (zklaic@gfz.hr). Authors are not authorized to publicly share meteorological data. To access these data, requests should be sent to the Croatian Meteorological and Hydrological Service.

Financial support

This study was supported by the project "Hydrodynamic Modeling of Plitvice Lakes System" (PLNP; grant no. 7989/16).

Author contributions

KŠ designed the model, wrote the model code, ran the simulations and performed the result post processing. ZBK organized the lake temperature experiment and contributed to the model development and the result evaluation and interpretation. Both authors contributed to the discussion and writing of the paper.

Competing interests

The authors declare that they have no conflicts of interest.

Acknowledgments

This study was performed under the project "Hydrodynamic Modeling of Plitvice Lakes System" founded by the Plitvice Lakes National Park, Croatia (PLNP; grant no. 7989/16). We also appreciate the technical support of the PLNP during equipment installation and lake temperature data acquisition. Meteorological data were provided by the Croatian Meteorological and Hydrological Service. A 2019 bathymetry experiment was organized by the PLNP. Melita Burić of Gekom – Geophysical and ecological modeling Ltd., Zagreb, Croatia produced composite pictures of the lake bathymetries and the digital orthophoto images.

References

Bahr, A., Evans, C., Martinoli, A., Huwald, H., Higgins, C. and Parlange, M.: Measuring sensible heat flux with high spatial density, in 2012 IEEE Sensors Applications Symposium Proceedings, SAS 2012, Brescia, Italy, 7-9 February 2012, 255–260, 2012.

Bell, V. A., George, D. G., Moore, R. J. and Parker, J.: Using a 1-D mixing model to simulate the vertical flux of heat and oxygen in a lake subject to episodic mixing, Ecol. Modell., 190, 41–54, doi:10.1016/j.ecolmodel.2005.02.025, 2006.

Benson, B. B., and Krause Jr., D.: The concentration and isotopic fractionation of gases dissolved in freshwater in equilibrium with the atmosphere. 1. Oxigen, Limnol. Oceanogr., 25(4), 662–671, doi:10.4319/lo.1980.25.4.0662, 1980.

Bolton, D.: The computation of equivalent potential temperature, Mon. Weather Rev., 108(7), 1046–1053, doi:10.1175/1520-0493(1980)108<1046:TCOEPT>2.0.CO;2, 1980.

Bourges, B.: Improvement in solar declination computation, Sol. Energy, 35(4), 367–369, doi:10.1016/0038-092X(85)90144-6, 1985.

https://doi.org/10.5194/gmd-2021-118
Preprint. Discussion started: 16 June 2021

Bristow, K. L. and Campbell, G. S.: On the relationship between incoming solar radiation and daily maximum and minimum temperature, Agric. For. Meteorol., 31, 159–166, doi:10.1016/0168-1923(84)90017-0, 1984.

Bruce, L. C., Frassl, M. A., Arhonditsis, G. B., Gal, G., Hamilton, D. P., Hanson, P. C., Hetherington, A. L., Melack, J. M., Read, J. S., Rinke, K., Rigosi, A., Trolle, D., Winslow, L., Adrian, R., Ayala, A. I., Bocaniov, S. A., Boehrer, B., Boon, C., Brookes, J. D., Bueche, T., Busch, B. D., Copetti, D., Cortés, A., de Eyto, E., Elliott, J. A., Gallina, N., Gilboa, Y., Guyennon, N., Huang, L., Kerimoglu, O., Lenters, J. D., MacIntyre, S., Makler-Pick, V., McBride, C. G., Moreira, S., Özkundakci, D., Pilotti, M., Rueda, F. J., Rusak, J. A., Samal, N. R., Schmid, M., Shatwell, T., Snorthheim, C., Soulignac, F., Valerio, G., van der Linden, L., Vetter, M., Vinçon-Leite, B., Wang, J., Weber, M., Wickramaratne, C., Woolway, R. I., Yao, H. and Hipsey, M. R.: A multi-lake comparative analysis of the General Lake Model (GLM): Stress-testing across a global observatory network, Environ. Model. Softw., 102, 274–291, doi:10.1016/j.envsoft.2017.11.016, 2018.

Brunel, J. P.: Estimation of sensible heat flux from measurements of surface radiative temperature and air temperature at two meters: Application to determine actual evaporation rate, Agric. For. Meteorol., 46, 179–191, doi:10.1016/0168-1923(89)90063-4, 1989.

Brutsaert, W.: On a Derivable Formula for Long-Wave Radiation From Clear Skies FLD), Water Resour. Res., 11(5), 742–744, doi:10.1029/wr011i005p00742, 1975.

Bryan, A. M., Steiner, A. L. and Posselt, D. J.: Regional modeling of surface-atmosphere interactions and their impact on Great Lakes hydroclimate, J. Geophys. Res. Atmos., 120(3), 1044–1064, doi:10.1002/2014JD022316, 2015.

Crawford, T. M. and Duchon, C. E.: An improved parameterization for estimating effective atmospheric emissivity for use in calculating daytime downwelling longwave radiation, J. Appl. Meteorol., 38(4), 474–480, doi:10.1175/1520-0450(1999)038<0474:AIPFEE>2.0.CO;2, 1999.

Forcat, F., Roget, E., Figueroa, M., and Sánchez, X.: Earth rotation effects on the internal wave field in a stratified small lake: Numerical simulations, Limnetica, 30(1), 27–42, doi:10.23818/limn.30.04, 2011.

Goudsmit, G. H., Burchard, H., Peeters, F. and Wüest, A.: Application of k-ε turbulence models to enclosed basins: The role of internal seiches, J. Geophys. Res., 107(C12), (23-1)-(23-13), doi:10.1029/2001jc000954, 2002.

Henderson-Sellers, B.: New formulation of eddy diffusion thermocline models, Appl. Math. Model., 9(6), 441–446, doi:10.1016/0307-904X(85)90110-6, 1985.

Hipsey, M. R., Bruce, L. C., Boon, C., Busch, B., Carey, C. C., Hamilton, D. P., Hanson, P. C., Read, J. S., De Sousa, E., Weber, M. and Winslow, L. A.: A General Lake Model (GLM 3.0) for linking with high-frequency sensor data from the Global Lake Ecological Observatory Network (GLEON), Geosci. Model Dev., 12(1), 473–523, doi:10.5194/gmd-12-473-2019, 2019.

Hostetler, S. W. and Bartlein, P. J.: Simulation of lake evaporation with application to modeling lake level variations of Harney-Malheur Lake, Oregon, Water Resour. Res., 26(10), 2603–2612, doi:10.1029/WR026i010p02603, 1990.

https://doi.org/10.5194/gmd-2021-118
Preprint. Discussion started: 16 June 2021

Klaić, Z. B. and Kvakić, M.: Modeling the impacts of the man-made lake on the meteorological conditions of the surrounding areas, J. Appl. Meteorol., 53, 1121–1142, https://doi.org/10.1175/JAMCD-13-0163.1, 2014.

Klaić, Z. B., Rubinić, J. and Kapelj, S.: Review of research on Plitvice Lakes, Croatia in the fields of meteorology, climatology, hydrology, hydrogeochemistry and physical limnology, Geofizika, 35, 189–278, doi:10.15233/gfz.2018.35.9, 2018.

Klaić, Z. B., Babić, K. and Mareković, T.: Internal seiches in a karstic mesotrophic lake (Prošće, Plitvice Lakes, Croatia), Geofizika, 37, 1–32, doi:10.15233/gfz.2020.37.11, 2020a.

Klaić, Z. B., Babić, K. and Orlić, M.: Evolution and dynamics of the vertical temperature profile in an oligotrophic lake, Hydrol. Earth Syst. Sci., 24(7), 3399–3416, doi:10.5194/hess-24-3399-2020, 2020b.

Kristovich, D. R., Clark, R. D., Frame, J., Geerts, B., Knupp, K. R., Kosiba, K. A., Laird, N. F., Metz, N. D., Minder, J. R., Sikora, T. D., Steenburgh, W. J., Steiger, S. M., Wurman, J. and Young, G. S.: The Ontario winter lake-effect systems field campaign: Scientific and educational adventures to further our knowledge and prediction of lake-effect storms, Bull. Am. Meteorol. Soc., 98(2), 315–332, doi:10.1175/BAMS-D-15-00034.1, 2017.

Krumgalz, B. S.: Temperature Dependence of Mineral Solubility in Water. Part 3. Alkaline and Alkaline Earth Sulfates, J. Phys. Chem. Ref. Data, 47(2), doi:10.1063/1.5031951, 2018.

Kudish, A. I. and Evseev, E.: Statistical relationships between solar UVB and UVA radiation and global radiation measurements at two sites in Israel, Int. J. Climatol., 20(7), 759–770, doi:10.1002/1097-0088(20000615)20:7<759::AID-JOC494>3.0.CO;2-K, 2000.

Kudish, A. I., Lyubansky, V., Evseev, E. G. and Ianetz, A.: Inter-comparison of the solar UVB, UVA and global radiation clearness and UV indices for Beer Sheva and Neve Zohar (Dead Sea), Israel, Energy, 30(9 SPEC. ISS.), 1623–1641, doi:10.1016/j.energy.2004.04.033, 2005.

Ladwig, R., Hanson, P., Dugan, H. A., Carey, C. C., Zhang, Y., Shu, L., Duffy, C. J., and Cobourn, K. M.: Lake thermal structure drives interannual variability in summer anoxia dynamics in a eutrophic lake over 37 years, Hydrol. Earth Syst. Sci., 25, 1009–1032, doi:10.5194/hess-25-1009-2021, 2021.

Liston, G. E. and Hall, D. K.: An energy-balance model of lake-ice evolution, J. Glaciol., 41(138), 373–382, doi:10.3189/S0022143000016245, 1995.

MacKay, M. D.: A process-oriented small lake scheme for coupled climate modeling applications, J. Hydrometeorol., 13(6), 1911–1924, doi:10.1175/JHM-D-11-0116.1, 2012.

MacKay, M. D., Verseghy, D. L., Fortin, V., and Rennie, M. D.: Wintertime simulations of a boreal lake with the Canadian Small Lake Model, J. Hydrometeorol., 18, 2143–2160, doi:10.1175/JHM-D-16-0268.1, 2017.

Martynov, A., Sushama, L., and Laprise, R.: Simulation of temperate freezing lakes by one-dimensional lake models: performance assessment for interactive coupling with regional climate models, Boreal Env. Res, 15, 143–164, 2010.

Mironov, D., Heise, E., Kourzeneva, E., Ritter, B., Schneider, N. and Terzhevik, A.: Implementation of the lake parameterisation scheme FLake into the numerical weather prediction model COSMO, Boreal Environ. Res., 15, 218–230, 2010.

https://doi.org/10.5194/gmd-2021-118
Preprint. Discussion started: 16 June 2021

690 Monin, A.S., Obukhov, A.M.: Basic laws of turbulent mixing in the surfacelayer of the atmosphere. Tr. Akad. Nauk SSSR Geophiz. Inst., 151, 163–187, 1954.

NIWA, Latent and sensible heat fluxes from lake water surfaces: https://niwa.co.nz/our-services/software/heat-fluxes-from-lakes/ last access: 28 January 2021.

NPPL (National Park Plitvička Jezera): https://np-plitvicka-jezera.hr/en/scientific-research/historical-overview/ last access: 24
695 January 2021.

Pashiardis, S., Kalogirou, S. and Pelengaris, A.: Statistical Analysis and Inter- Comparison of Solar UVB and Global Radiation for Athalassa and Larnaca, Cyprus, SM J. Biometrics Biostat., 2(2), 1012, doi:10.36876/smjbb.1006, 2017.

Podstawczynska, A.: UV and global solar radiation in Łodz, Central Poland, Int. J. Climatol., (30), 1–10, doi:10.1002/joc.1864, 2009.

700 Pokhrel, R. P. and Bhattarai, B. K.: Relation between Global Solar Radiation and Solar Ultraviolet Radiation in Different Parts of Nepal, J. Inst. Eng., 8(3), 169–175, doi:10.3126/jie.v8i3.5942, 2012.

Rasconi, S., Winter, K., and Kainz, M. J.: Temperature increase and fluctuation induce phytoplankton biodiversity loss – Evidence from a multi-seasonal mesocosm experiment, Ecol. Evol., 7:2936–2946, 10.1002/ece3.2889, 2017.

Stefan, H. G., Fang, X. and Hondzo, M.: Simulated climate change effects on year-round water temperatures in temperate zone
705 lakes, Clim. Change, 40, 547–576, doi:10.1023/A:1005371600527, 1998.

Stepanenko, V. M., Machulskaya, E. E., Glagolev, M. V. and Lykossov, V. N.: Numerical modeling of methane emissions from lakes in the Permafrost Zone, Izv. - Atmos. Ocean Phys., 47(2), 252–264, doi:10.1134/S0001433811020113, 2011.

Stepanenko, V. M., Martynov, A., Jöhnk, K. D., Subin, Z. M., Perroud, M., Fang, X., Beyrich, F., Mironov, D. and Goyette,
710 S.: A one-dimensional model intercomparison study of thermal regime of a shallow, turbid midlatitude lake, Geosci. Model Dev., 6(4), 1337–1352, doi:10.5194/gmd-6-1337-2013, 2013.

Stepanenko, V., Jöhnk, K. D., Machulskaya, E., Perroud, M., Subin, Z., Nordbo, A., Mammarella, I. and Mironov, D.: Simulation of surface energy fluxes and stratification of a small boreal lake by a set of one-dimensional models, Tellus, Ser. A Dyn. Meteorol. Oceanogr., 66, 1–18, doi:10.3402/tellusa.v66.21389, 2014.

715 Stepanenko, V., Mammarella, I., Ojala, A., Miettinen, H., Lykosov, V. and Vesala, T.: LAKE 2.0: A model for temperature, methane, carbon dioxide and oxygen dynamics in lakes, Geosci. Model Dev., 9(5), 1977–2006, doi:10.5194/gmd-9-1977-2016, 2016.

Sun, S., Yan, J., Xia, N. and Sun, C.: Development of a Model for Water and Heat Exchange Between the Atmosphere and a Water Body, Adv. Atmos. Sci., 24(5), 927–938, doi:10.1007/s00376-007-0927-7, 2007.

720 Thiery, W., Martynov, A., Darchambeau, F., Descy, J. P., Plisnier, P. D., Sushama, L. and Van Lipzig, N. P. M.: Understanding the performance of the FLake model over two African Great Lakes, Geosci. Model Dev., 7(1), 317–337, doi:10.5194/gmd-7-317-2014, 2014.

https://doi.org/10.5194/gmd-2021-118
Preprint. Discussion started: 16 June 2021

Vachon, D., Langenegger, T., Donis, D. and McGinnis, D. F.: Influence of water column stratification and mixing patterns on the fate of methane produced in deep sediments of a small eutrophic lake, Limnol. Oceanogr., 64(5), 2114–2128, doi:10.1002/lno.11172, 2019.

Verburg, P. and Antenucci, J. P.: Persistent unstable atmospheric boundary layer enhances sensible and latent heat loss in a tropical great lake: Lake Tanganyika, J. Geophys. Res. Atmos., 115(11), 1–13, doi:10.1029/2009JD012839, 2010.

Vinnå, L. R., Medhaug, I., Schmid, M. and Bouffard, D.: The vulnerability of lakes to climate change along an altitudinal gradient, Nat. Commun. Earth Environ., 2(1), 1–10, doi:10.1038/s43247-021-00106-w, 2021.

Wald, L.: Basics in Solar radiation at Earth's surface, hal-02164311, 2019.

Wang, K. and Dickinson, R. E.: Global Atmospheric Downward Longwave Radiation at the Surface From Ground-Based Observations, Satellite Retrievals, and Reanalyses, Rev. Geophys., (51), 150–185, doi:10.1002/rog.20009, 2013.

Willmott, C. J. and Matsuura, K.: Advantages of the mean absolute error (MAE) over the root mean square error (RMSE) in assessing average model performance, Clim. Res., 30(1), 79–82, doi:10.3354/cr030079, 2005.

Willmott, C. J., Robeson, S. M. and Matsuura, K.: A refined index of model performance, Int. J. Climatol., 32(13), 2088–2094, doi:10.1002/joc.2419, 2012.

Winslow, J. C., Hunt, E. R. and Piper, S. C.: A globally applicable model of daily solar irradiance estimated from air temperature and precipitation data, Ecol. Modell., 143(3), 227–243, doi:10.1016/S0304-3800(01)00341-6, 2001.

Wu, Y., Huang, A., Yang, B., Dong, G., Wen, L., Lazhu, Zhang, Z., Fu, Z., Zhu, X., Zhang, X. and Cai, S.: Numerical study on the climatic effect of the lake clusters over Tibetan Plateau in summer, Clim. Dyn., 53, 5215–5236, doi:10.1007/s00382-019-04856-4, 2019.

Wu, Y., Huang, A., Lazhu, Yang, X., Qiu, B., Wen, L., Zhang, Z., Fu, Z., Zhu, X., Zhang, X., Cai, S. and Tang, Y.: Improvements of the coupled WRF-Lake model over Lake Nam Co, Central Tibetan Plateau, Clim. Dyn., 55(9–10), 2703–2724, doi:10.1007/s00382-020-05402-3, 2020.